Climate sensitivity of the summer runoff of two glacierised Himalayan catchments with contrasting climate

Sourav Laha[1,2], **Argha Banerjee**[1], **Ajit Singh**[2], **Parmanand Sharma**[2], **and Meloth Thamban**[2]

[1]Earth and Climate Science, Indian Institute of Science Education and Research (IISER) Pune, Pune-411008, India
[2]National Centre for Polar and Ocean Research (NCPOR), Ministry of Earth Sciences, Vasco-da-Gama, Goa-403804, India

Correspondence: Argha Banerjee (argha@iiserpune.ac.in)

Abstract. The future changes in runoff of Himalayan glacierised catchments will be determined by the local climate forcing and the climate sensitivity of the runoff. Here, we investigate the sensitivity of summer runoff to precipitation and temperature changes in winter-snow dominated Chandra (the western Himalaya) and summer-rain dominated upper Dudhkoshi (the eastern Himalaya) catchments. We analyse the interannual variability of summer runoff in these catchments during 1980–2018 using a semi-distributed glacio-hydrological model, which is calibrated with the available runoff and glacier mass balance observations. Our results indicate that despite the contrasting precipitation regimes, the catchments have a similar runoff response: The summer runoff from the glacierised parts of both the catchments is sensitive to temperature changes and is insensitive to precipitation changes; the summer runoff from the non-glacierised parts of the catchments has an exactly opposite pattern of sensitivity. The precipitation-independent glacier contribution stabilises the catchment runoff against precipitation variability to some degree. The estimated sensitivities capture the characteristic 'peak water' in the long-term mean summer runoff, which is caused by the excess meltwater released by the shrinking ice reserve. As the glacier cover depletes, the summer runoff is expected to become more sensitive to precipitation forcing in these catchments. However, The net impact of the glacier loss on the catchment runoff may not be detectable, given the relatively large interannual runoff variability in these catchments.

1 Introduction

The presence of glaciers in a catchment significantly influences the diurnal to seasonal to interannual variability of the runoff, and its long-term multidecadal changes (Hock et al., 2005). Himalayan glacier-fed rivers play a key part in sustaining the downstream population and ecosystem (Azam et al., 2021). It is important to analyse the potential catchment-scale hydrological changes in the Himalaya as a significant reduction in the regional glacier cover by 2100 is expected (Kraaijenbrink et al., 2017). This problem has motivated several glacio-hydrological model studies of the Himalayan basins and catchments (see Azam et al. (2021) for a review). These models often differ from each other in the level of descriptions of glacial processes, e.g., no explicit treatment of the glaciers (Pokhrel et al., 2014), a static (Nepal, 2016), or dynamic (Kraaijenbrink et al., 2017) glacier cover, a simple temperature-index (Chandel and Ghosh, 2021; Banerjee, 2022) or energy-balance based ice-melt model (Fujita and Sakai, 2014), and so on. Even a single model, when tuned with different available baseline climate data products, predicts a wide range of future hydrological changes (Koppes et al., 2015). In addition, the available future climate projections used to drive the glacio-hydrological models have a large spread (Sanjay et al., 2017). All of the above factors contribute to a wide range of predictions for the future changes in the runoff of Himalayan catchments (e.g. Nie et al., 2021). Assessing climate sensitivity of the runoff of Himalayan catchments may prove useful in reconciling the range of predictions available in the literature. Climate sensitivity of runoff is defined as the change in runoff due to a unit perturbation in a forcing variable, e.g., precipitation or temperature (Zheng et al., 2009). The climate sensitivities estimated from different models, which are forced by different projected climate forcing, can therefore be compared (Vano et al., 2012). A climate sensitivity analysis may also reveal key differences and similarities in the climate response of runoff generated from the different parts of a catchment

(Banerjee, 2022) that are dominated by either snow melt or glacier melt or rainfall (Fujita and Sakai, 2014). It may also bring out the similarities and the differences among catchments across the Himalayan arc with their distinct climate settings, and thus, provide a better handle on the runoff response in the ungauged catchments in this data-sparse region (Azam et al., 2021).

In the literature, climate-sensitivities have been used to estimate long-term runoff changes due to temperature and precipitation forcing in both glacierised (Chen and Ohmura, 1990) and non-glacierised catchments (Dooge et al., 1999; Zheng et al., 2009; Vano et al., 2012). In the Himalaya, climate sensitivity of glacier mass balance proved useful to explain the observed spatial pattern of glacier thinning (Sakai and Fujita, 2017; Kumar et al., 2019), or to identify an inherent bias in scaling-based glacier evolution models which are often used in glacio-hydrological studies (Banerjee et al., 2020). A recent study used a simple temperature-index model to establish a weak precipitation sensitivity of glacier runoff in general (Banerjee, 2022).

Despite its potential utility, detailed studies of the climate sensitivity of the runoff of Himalayan glacierised catchments are limited (Fujita and Sakai, 2014; Azam and Srivastava, 2020). Motivated by this gap, the present study uses a detailed process-based glacio-hydrological model to explore the sensitivity of glacier and off-glacier summer runoff, and to analyse the underlying mechanisms driving the sensitivities. Note that throughout the paper, the annual quantities correspond to the hydrological year from 1st October of a calendar year to 30th September of the next, and summer season refers to the period from 1st May to 30th September (e.g., Azam et al., 2019). Also, runoff of a catchment implies the streamflow at the catchment outlet, and glacier (off-glacier) runoff denotes the contribution of the glacierised (glacier-free) areas of the catchment to the streamflow. We study two contrasting glacierised Himalayan catchments: winter-precipitation dominated Chandra (the western Himalaya), and summer-precipitation dominated upper Dudhkoshi (the eastern Himalaya). Climate sensitivities of runoff can be obtained simply by regressing the observed variability of runoff to those of its meteorological drivers (e.g. Zheng et al., 2009). When observations are not available, model simulations can be used for the same (Vano et al., 2012). Here, we use the Variable Infiltration Capacity (VIC) model (Liang et al., 1996) augmented with a glacier-melt module, to simulate runoff of the studied catchment over the period 1980–2018. The simulated runoff is used to estimate and validate the sensitivities of summer runoff to annual precipitation and summer temperature. The sensitivities of the runoff of the glacierised and non-glacierised parts of the catchments are also analysed separately. These sensitivities are then used to understand the multidecadal changes in the mean and the variability of summer runoff of the two catchments, as the glaciers shrink in a warming climate.

2 Study area

We considered two high Himalayan catchments with contrasting climate regimes: Chandra (Indus basin, the western Himalaya), and upper Dudhkoshi (Ganga basin, the eastern Himalaya) (Figs. 1 and 2). Chandra catchment is in Lahaul-Spiti district, Himachal Pradesh, India. Upper Dudhkoshi catchment is located in Solukhumbu district of Nepal. The mean annual precipitation is similar in both the catchments, but its seasonality is different. About 70% of the annual precipitation in Chandra catchment occurs during the winter months (Fig. 1c) due to the Western Disturbances (Azam et al., 2019), and the influence of the Indian summer monsoon is relatively weak. In upper Dushkoshi catchment, more than 80% of the precipitation happens during the summer months (Fig. 1c) with a dominant influence of the Indian summer monsoon. Consequently, glacier accumulation mainly occurs during winter (summer) months in Chandra (upper Dudhkoshi) catchment. Due to the contrasting seasonality of precipitation, the ratio of liquid to solid precipitation in Chandra and upper Dudhkoshi catchments are 0.5 and 9.7, respectively (Table 1). The catchment area of upper Dudhkoshi is approximately half of Chandra catchment. The glacierised fraction in Chandra catchment is 20% higher than that of upper Dudhkoshi. The mean annual temperature is 0.8°C lower in Chandra catchment compared to upper Dudhkoshi catchment. However, the former has a more pronounced seasonality with a warmer summer and a cooler winter (Fig. 1d). Chandra catchment has a somewhat higher annual and summer runoff. Some important characteristics of the two catchments are compared in Table 1.

3 Data and methods

Below we present methodological details related to the input data, the glacio-hydrological model, and the climate sensitivity analysis.

3.1 Hydro-meteorological and glaciological data

3.1.1 Observations

Observed hourly runoff of Chandra river at Tandi (32.55°N, 76.97°E, 2850 m a.s.l.) from 26th June, 2016 to 30th Oct, 2018 was available for three summer seasons with some data gaps (Fig. 5b) (Singh et al. (2020); supplementary Table S1). Hourly 2m air temperature, precipitation, and incoming shortwave radiation were measured at the Himansh station (32.409°N, 77.609°E, 4080 m a.s.l.) in the catchment between 18th October, 2015 to 5th October, 2018 with some data gaps (Oulkar et al. (2022), supplementary Table S1).

Hourly runoff from upper Dudhkoshi catchment was observed at Phadking (27.74°N, 86.71°E, 2600 m a.s.l.) between 7th April, 2010 and 16th April, 2017 (Fig. 5a) (Chevallier et al., 2017). Available hourly air temperature and precip-

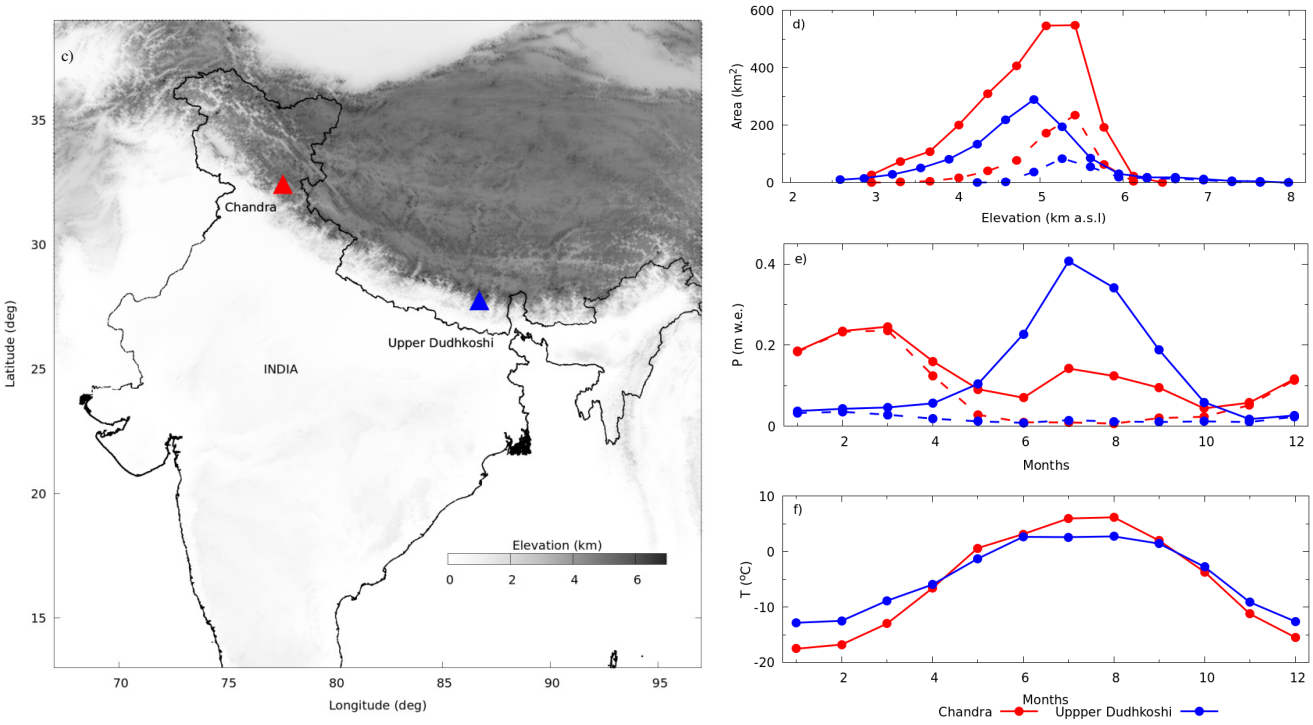

Figure 1. a) The location of Chandra (red solid triangle) and upper Dudhkoshi (blue solid triangle) catchments on a grey-scale elevation map (Amante et al., 2009). In the rest of the plots red (blue) colors refer to Chandra (upper Dudhkoshi) catchment. The solid magenta (sky-blue) polygon shows Ganga (Indus) basin. b) Area-elevation distribution of the catchments (solid lines + solid symbols), and that of the glacierised parts (dashed lines + solid symbols). c) Mean monthly precipitation (solid lines + solid symbols), along with the monthly snowfall (dashed lines + solid symbols). d) Mean monthly temperature profiles (solid lines + solid symbols).

Table 1. A summary of the characteristics of Chandra and upper Dudhkoshi catchments. The meteorological variables are bias-corrected reanalysis data averaged over the catchments (Hersbach et al., 2020), the hydrological data are from model simulations (the present study). The glacier mass-balance and area-loss estimates are from the existing literature (supplementary Table S3).

Catchment	Chandra	Upper Dudhkoshi
Basin	Indus	Ganga
Area (km^2)	2440	1190
Outlet	Tandi	Phadking
Elevation range (m a.s.l)	2850–6500	2600–7900
Glacierised fraction	0.25	0.20
Annual temperature ($^\circ$C)	-5.5	-4.7
Annual precipitation (m yr^{-1})	1.6	1.5
Summer precipitation / winter precipitation	0.5	6.8
Liquid precipitation/ solid precipitation	0.5	9.7
Glacier area loss (% $decade^{-1}$)	1.1–5.5	1.2–4.2
Glacier mass balance (m w.e. yr^{-1})	-0.13 ± 0.11 to -0.56 ± 0.38	-0.26 ± 0.13 to -0.52 ± 0.22
Annual runoff (m yr^{-1})	1.25	0.99
Summer runoff/annual runoff	0.86	0.81

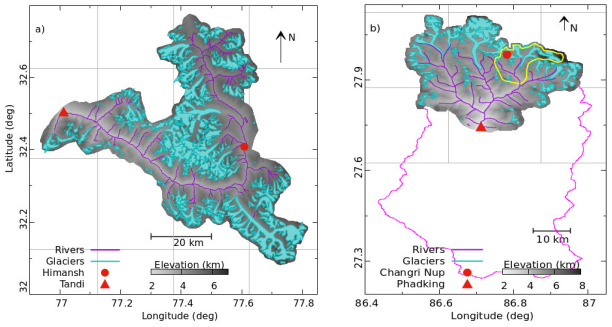

Figure 2. Maps of (a) Chandra and (b) upper Dudhkoshi catchments showing glaciers (Cyan polygons) and streams (purple lines). The red solid circles (triangles) are the meteorological (hydrological) stations. The ERA5 grid boxes are shown with solid gray lines in the background. Solid magenta and yellow polygons show Dudhkoshi and Periche catchments.

itation data at Phadking from 7th April, 2010 to 23th April, 2017 (with some data gaps) (Chevallier et al., 2017) were used. The daily incoming shortwave radiation data for the period 1st November, 2010 to 30th November, 2014 at nearby Changri Nup station (27.983°N, 86.783°E, 5400 m a.s.l.) in the same catchment were used (Sherpa et al. (2017); supplementary Table S1).

We considered eight available geodetic mass-balance observations that spanned a decade or more, for each of the catchments (supplementary Table S3). Randolph Glacier Inventory (RGI 6) (Arendt et al., 2017) was used for the glacier boundaries that corresponded to the glacier extent in 2002.

3.1.2 Reanalysis data and bias correction

We used hourly 2-m air temperature, precipitation, and windspeed from fifth-generation European Center for Medium-Range Weather Forecasts Atmospheric Reanalysis of the global climate (ERA5) from 1980 to 2018 (Hersbach et al., 2020) to force the VIC model at a spatial resolution of 0.25°×0.25°. Following the existing hydrological studies of various high Himalayan catchments (Soncini et al., 2016; Azam and Srivastava, 2020), the temperature data were bias-corrected. The available observed air-temperature data at the Himansh station (Chandra catchment), and at Phadking (Dudhkoshi Catchment) were used to compute the mean monthly temperature biases (supplementary Fig. S1), assumed to be constant for the whole catchment and over the whole simulation period.

To compute temperature at any given elevation within a grid box, mean monthly lapse rates (supplementary Fig. S2) were used. In Chandra catchment, the lapse rates were computed at the grid box containing Himansh station using ERA5 temperature from the four near-neighbour grid boxes. The corresponding annual lapse rate of 4.7±1.2 °C km^{-1} was consistent with previously observed values of 4.4–6.4 °C km^{-1} (Azam et al., 2019; Pratap et al., 2019). In upper Dudhkoshi catchment, the monthly lapse rates derived from ERA5 were significantly larger than those observed between Phadking and Changri Nup stations over the period 2013–2016, so we used the observed lapse rates. The corresponding mean annual lapse rate of 4.6±0.6 °C km^{-1} in this catchment was the same as that previously reported (Pokhrel et al., 2014).

ERA5 precipitation data was corrected by scaling with a catchment-specific constant α_P for each of the catchments following the existing studies from the region (Huss and Hock, 2015; Bhattacharya et al., 2019; Azam and Srivastava, 2020). The scale factor, which ensured water balance over the catchments, was calibrated using the observed runoff and glacier mass-balance employing a Bayesian procedure (see Sect. 3.2.3). In some of the existing studies in the region, an elevation-dependent precipitation scaling has also been employed (e.g., Azam et al., 2019). However, as an elevation-dependent correction may potentially introduce additional uncertainties (e.g., Johnson and Rupper, 2020), we preferred a constant α_p keeping the number of calibration parameters to a minimum. Note that the precipitation biases over the rugged Himalayan catchments (∼1000 km^2) cannot be accurately corrected using data from a single station because of a high spatial variability and a small correlation length associated with precipitation (Singh and Kumar, 1997).

We scaled the incoming shortwave radiation obtained from VIC model by a catchment-specific constant to match the corresponding mean values observed at Himansh (Chandra catchment) and Changri Nup (upper Dudhkoshi catchment) stations (supplementary Fig. S3).

3.2 Glacio-hydrological model setup

We divided each studied catchment into two parts, the glacierised and non-glacierised ones. On the non-glacierised part, we ran another VIC model (Liang et al., 1996) to compute the surface runoff, baseflow, and evapotranspiration at hourly time steps (Fig. 3). On the glacierised part, a separate VIC model run at hourly time steps was used to get the snow melt, and a temperature-index model (Hock, 2003) was used to obtain the glacier melt (Fig. 3). The additional glacier module was needed as VIC model does not have the capability to compute glacier melt (Liang et al., 1996). A similar approach to represent glacier melt was used in existing VIC model studies in the region (Zhang et al., 2013; Zhao et al., 2015; Chandel and Ghosh, 2021). Hourly hydrological fluxes of the non-glacierised and glacierised parts within each gridbox were combined and routed (Lohmann et al., 1998) to obtain the total runoff at the catchment outlet. In this step, the flow from each gridbox was partitioned into the fast and slow components using hydrographs parameterised with Bf and Ks, UH^F_{max}, and UH^F_{pow} (Lohmann et al., 1998). The total hourly runoff produced from each grid box was routed

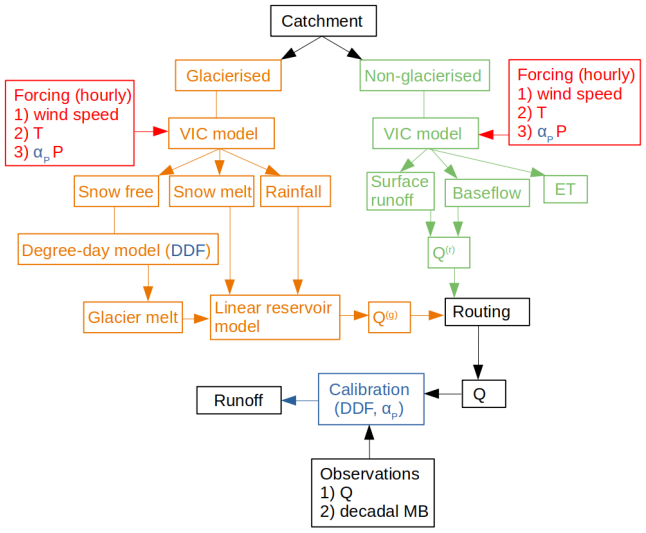

Figure 3. Flow chart of the glacio-hydrological model setup (see Sect. 3.2 for details).

downstream in the direction of steepest descent using a linearised Saint-Venant equation (Lohmann et al., 1998).

3.2.1 Hydrological model

VIC (version 4.2.d, accessible from https://vic.readthedocs.io/en/master/; Liang et al. (1996)) is a semi-distributed macro-scale hydrological model, which simulates the fluxes of water and energy for a grid-based representation of a catchment using physically-based parameterisations of hydrological processes (Liang et al., 1996). In this model, water can enter a gridbox only from the atmosphere, and once water reaches the river channel, it can not flow back into the gridbox. These assumptions limit the applicability of the model to a larger grid size (e.g., a grid size of 0.25° which was used here). The VIC model considers sub-grid heterogeneity in surface topography, land-cover, and sub-surface soil properties. Different vegetation classes are represented by tiles covering a fraction of the gridbox, and an area-weighted sum over the tiles obtains various hydrological fluxes for each gridbox. VIC model partitions the input precipitation at each gridbox into rain and snow based on a threshold temperature T_{th}. It uses a two-layered snowpack, computing the snow melt at a given elevation with an energy-balance approach. A surface-albedo parameterisation incorporating the effects of snowfall and aging of snow, snow-sublimation, and refreezing of meltwater within the snowpack are included in the model (Andreadis et al., 2009). Evapotranspiration is computed by Penman-Monteith equation (Liang et al., 1996) as the sum of canopy evaporation, bare soil evaporation, and transpiration for each vegetation class. VIC allows multiple subsurface soil layers, and here we used three of them. The partitioning between surface runoff and infiltration into the top layer is done using a variable infiltration curve (Liang et al., 1996) controlled by the parameter b_{inf}. The bottom layer produces the baseflow depending on the moisture content with a maximum allowed baseflow of Ds_{max}. At low soil moisture (below a fraction Ws of the maximum allowed soil moisture, and up to a fraction Ds of Ds_{max}), the baseflow is linear in it. Beyond this linear regime, a non-linear ARNO recession curve determines baseflow (Liang et al., 1996). The chosen values of the above five VIC model parameters are given in supplementary Table S2.

Dictated by the resolution of ERA5 input data, the model was run at a 0.25° × 0.25° spatial resolution and at an hourly time steps. Chandra (upper Dudhkoshi) catchment covered parts of 11 (6) ERA5 grid boxes (Figs. 2a–2b), with fractional grid cover in the range 2.5–92% (2–68%). The static input parameters included soil properties (Fischer et al., 2008), land use (Friedl and Sulla, 2019), vegetation information (Rodell et al., 2004), and elevation distribution (Farr et al., 2007) for each gridbox. We used 10 elevation bands with width in the range 100–300 m depending on the elevation range within the gridbox. A minimal set of meteorological forcing parameters, namely, bias-corrected air temperature, scaled precipitation, and wind speed from ERA5 reanalysis (Hersbach et al., 2020) over the period 1980–2018 were used to force the model. For model spin-up, we extended the meteorological input data back by repeating the data from 1980 to 1984.

3.2.2 Glacier model

On the glacierised grids of each catchment, a separate VIC model computed the snow melt and snow-covered fraction of each elevation band (Fig. 3). A minimal temperature-index model (Hock, 2003) was chosen to simulate the ice melt over the corresponding snow-free areas. This one-parameter model is easy to calibrate and is expected to work well for ice cover than for snow cover, due to a relatively low seasonal variability of ice albedo (Hock, 2003). The glacier melt module was forced with the bias-corrected ERA5 air temperature, while taking into account the elevation of the band using a mean monthly lapse rate (supplementary Fig. S2). The degree-day factors (DDF) for each of the catchments were calibrated simultaneously against the observed glacier mass balance and catchment runoff using a Bayesian method (see Sect. 3.2.3). The snow melt, ice melt, and rainfall on the glaciers routed using a linear reservoir model (Hannah and Gurnell, 2001), obtained the glacier runoff. The model used two parallel reservoirs: a slow reservoir with time constant K_{slow} for routing the snowmelt, and a fast reservoir with time constant K_{fast} for routing the sum of the icemelt and the rainfall (e.g., Hannah and Gurnell, 2001). Catchment-wise glacier mass balance was computed by subtracting the total ice and snow melt from the total snowfall over the glacierised parts.

The present glacier module did not consider snow redistribution within or between the glacierised and the non-glacierised parts of the catchment via avalanching (Laha et al., 2017) or wind redistribution. We did not consider any baseflow contribution from the glacierised parts assuming the negligible permeability of the bedrock. Also, the present model did not consider the effect of supraglacial debris layer on melting as only 4–7% of the studied catchments consist of debris-covered ice (Scherler et al, 2018). A simple inclusion of the melt inhibiting effects of the debris layer (e.g. Azam and Srivastava, 2020) may not necessarily lead to improved estimation of subdebris melt. For example, the strong melt enhancements at the ice-cilffs/ponds on the debris-covered surface (e.g. Miles et al, 2022) are often ignored in these models. The available estimates of the extent (e.g. Herreid and Pellicciotti, 2020) and thickness estimates (e.g. Rounce et al., 2018) have large uncertainties as well. Here, we verified that a simplified sub-debris melt scheme (Azam and Srivastava, 2020), which does not consider the variation of debris thickness, induced only small ($\sim$3%) insignificant changes in the summer runoff compared to the corresponding uncertainties ($\sim$10%). The effect of wind and gravity driven snow-redistribution in the rugged Himalayan topography are also difficult to capture in any coarse-scale model like the present one. As we are calibrating the observed mass balance of glaciers and catchment runoff, it may take care of the effects of these two factors to some extent.

We assumed a static glacier cover here as the observed percentage loss of glacier area over the simulation period was small (1–5 % decade^{-1}) for both the catchments (Table 1). Biases due to such a static-glacier approximation were found to be small for another glacierised Himalayan catchment over the same period (Azam and Srivastava, 2020). A dynamic description of glaciers within the glacio-hydrological model is needed only for predicting the long-term changes in runoff when potential changes in glacier extent is large (e.g., Kraaijenbrink et al., 2017).

3.2.3 Model calibration

With the limited set of observations available for the studied catchments, calibrating a large number of tunable parameters may not ensure a better representation of the relevant processes (Jost et al., 2012), and may lead to over-fitting. It may also suffer from equifinality issue (Beven and Freer, 2001; Jost et al., 2012), where more than one parameter combinations reproduce the observed runoff. For example, in glacierised catchments, the same runoff output can be generated by models which use different combinations of the precipitation scale factor and DDF (Azam and Srivastava, 2020). These models will, however, yield different relative contributions of glaciers to the total runoff, and obtain different climate sensitivities. To avoid the possibility of overfitting, we calibrated only two model parameters: 1) precipitation scale factor α_P, and 2) DDF of ice. To ensure an unique best-fit pair of the above parameters, we simultaneously fitted the available summer runoff and glacier mass balance data (e.g. Van Tiel et al., 2020b) using a Bayesian procedure as discussed below. For the rest of the VIC model parameters, we used the central values of the recommended range (supplementary Table S2). Note that, these uncalibrated VIC model parameters values were similar to that of the corresponding calibrated values used in some of the studies from the region (e.g., Zhang et al., 2013; Zhao et al., 2015; Bhattacharya et al., 2019; Chandel and Ghosh, 2021). This suggested that the VIC model parameters used here to describe the two Himalayan catchments were representative ones. These model parameter values are listed in supplementary Table S2.

To calibrate for the parameters α_P and DDF, we used a Bayesian method (e.g., Tarantola, 2005). For given a set of available observations d and a set of model parameters θ, the posterior probability of the model parameters given the observations was,

$$p(\theta|d) \propto p(d|\theta)p(\theta). \tag{1}$$

Here $p(\theta)$ was the prior distribution of the model parameters α_P and DDF. We assumed a uniform prior distribution over the range of values reported over the High Mountain Asia: 0.7–2.5 for α_P (Huss and Hock, 2015; Bhattacharya et al., 2019; Azam and Srivastava, 2020), and 2–16 mm °C^{-1} day^{-1} for DDF (Singh et al., 2000; Nepal, 2016; Azam et al., 2019). The conditional probability $p(d|\theta)$ of the observations d given the model parameter θ was assumed to be a bivariate normal distribution (e.g., Rounce et al., 2020; Werder et al., 2020), i.e., a normally distributed residuals for both discharge and glacier mass balance,

$$p(d|\theta) \sim e^{-\frac{\sum_i (Q_i^{mod} - Q_i^{obs})^2}{2\sigma_Q}} \times e^{-\frac{\sum_j (b_j^{mod} - b_j^{obs})^2}{2\sigma_b}}. \tag{2}$$

Here the superscript obs and mod denoted the observed and modelled values, respectively. Here, Q_i was the weekly summer runoff, and the summation was over all the years with observed runoff data. The j-th observed regional geodetic glacier mass balance for each catchment was denoted by b_j. This summation was over eight such observations (Bolch et al., 2011; Gardelle et al., 2012; Nuimura et al., 2012; Vincent et al., 2013; Vijay and Braun, 2016; Brun et al., 2017; King et al., 2017; Mukherjee et al., 2018; Maurer et al., 2019; Shean et al., 2020) for each of the catchment as listed in the supplementary Table S3. The uncertainties $\sigma_Q = \sqrt{(\sigma_Q^{mod})^2 + (\sigma_Q^{obs})^2}$ and $\sigma_b = \sqrt{(\sigma_b^{mod})^2 + (\sigma_b^{obs})^2}$ incorporated the errors in the model (σ^{mod}) and the observation (σ^{obs}). Each of these errors was assumed to be a constant having the following values. σ_Q^{obs} was taken to be $\sim$20% of the mean summer runoff of the catchments, which is a conservative estimate given the previously reported 5% error discharge measured using the same method for other Himalayan catchments (e.g., Singh et al., 2005). For both the catchments σ_b^{obs} was taken to be 0.32 m w.e yr^{-1}, which was

the maximum uncertainty associated with the observed regional geodetic glacier mass balance used in this study (supplementary Table S3). The values of σ_Q^{mod} and σ_b^{mod} were taken 0.15 (0.17) m yr^{-1} and 0.24 (0.27) m w.e yr^{-1}, respectively for Chandra (upper Dudhkoshi) catchment. The model errors were computed using an ensemble of 104 model runs where either a single (26 models) or a pair (78 models) of model parameters out of the 13 listed in supplementary Table S2 were perturbed from the central value by $\pm 25\%$ of their expected range. In these runs, except for the perturbed parameter/s, the rest of the parameters were kept the central value of the corresponding ranges. For calibration, the two-dimensional parameter space was scanned with step sizes of 0.2 for α_P, and 0.5 mm °C^{-1} day^{-1} for DDF. This yielded an ensemble of $11 \times 29 = 319$ models for each catchment, with associated weight $p(\theta|d)$ as computed using Eq. (1).

3.2.4 Model validation, parameter sensitivity, and uncertainty

The results from the most-probable model were used for estimating summer runoff and its components, and glacier mass balance. All the relevant quantities were computed for all the 319 models in the ensemble, and the corresponding weighted standard deviations were used to obtain the 2σ uncertainties. To assess the model performance, the simulated mean summer runoff, decadal glacier mass balance, and glacier melt contribution were compared with the corresponding modelled and observed values previously reported in the region. As the observed runoff was available for only 3 to 7 years, all of it was utilised for the above calibration without any validation period. For upper Dudhkoshi catchment the calibration procedure was repeated using data from a set of four consecutive years, while the remaining three year's data were utilised for validation. This experiment was repeated four times with different choices of calibration period.

Parameter sensitivity of the best-fit model due to the uncertainties in the uncalibrated parameters were evaluated with the help of additional 22 simulations where one of the 11 uncalibrated glacio-hydrological model parameters (supplementary Table S2) was perturbed by $\pm 25\%$ of the range of corresponding recommended values. The sensitivity of summer runoff to these 11 parameters were computed at the corresponding optimal values of DDF and α_P. Perturbing the parameters one by one in the 11-d parameter space is similar to computing the multidimensional gradient in this space to understand the model sensitivity. An ensemble of 22 model outputs was generated where one of the above 11 uncalibrated parameters (supplementary Table S2) of the best-fit model perturbed by $\pm 25\%$. To look for possible interactions between parameters, 78 additional simulations were ran, where a chosen pair of parameters were simultaneously perturbed.

3.3 Climate sensitivity of summer runoff

The climate sensitivity of specific summer runoff Q (m yr^{-1}) is defined as the change in runoff due to a unit perturbation in a meteorological forcing parameter (e.g., Zheng et al., 2009). Here, we considered the sensitivity of summer runoff Q due to changes in annual precipitation P (m yr^{-1}) and mean summer temperature T (°C), as summer runoff was $81-86\%$ of the annual runoff in these catchments (Table 1). We did not consider the annual or winter temperature as it is the summer temperature that controls glacier melt (e.g., Pratap et al., 2019).

3.3.1 Climate sensitivities and summer runoff anomalies

The sensitivities of summer runoff relate (e.g., Zheng et al., 2009) the anomalies of summer runoff δQ (m yr^{-1}), annual precipitation δP (m), and summer air-temperature δT (°C) as follows.

$$\delta Q = s_P \delta P + s_T \delta T. \tag{3}$$

Here, precipitation sensitivity is denoted by $s_P \doteq \frac{\partial Q}{\partial P} = \frac{\partial \delta Q}{\partial P}$ (m yr^{-1} m^{-1}), and temperature sensitivity is denoted by $s_T \doteq \frac{\partial Q}{\partial T} = \frac{\partial \delta Q}{\partial T}$ (m yr^{-1} °C^{-1}). In Eq. (3), a possible bilinear interaction term proportional to $\delta T \delta P$ (Lang, 1986) was not considered. We confirmed this correction term, when included in the regression for the catchment studied, was not significant ($p < 0.05$). In order to estimate the sensitivities s_T and s_P (Eq. (3)), we regressed simulated time series of δQ for the catchments during 1997–2018 with the corresponding time series of δT and δP. The sensitivities estimated from the simulated δQ time series over 1997–2018 were validated using that during 1980–1996 by computing the corresponding Nash-Sutcliffe efficiency (NSE) and root mean squared error (RMSE).

We also considered the runoff from glacierised part of the catchments $Q^{(g)} \doteq Q_0^{(g)} + \delta Q^{(g)}$, and that from the non-glacierised part of the catchments $Q^{(r)} \doteq Q_0^{(r)} + \delta Q^{(r)}$. Here, the notations Q_0 and δQ denote the long-term mean and the anomaly for a given year, respectively. The corresponding sensitivities were defined in a similar way and led to the relations,

$$\delta Q^{(g)} = s_P^{(g)} \delta P + s_T^{(g)} \delta T, \tag{4}$$

$$\delta Q^{(r)} = s_P^{(r)} \delta P + s_T^{(r)} \delta T. \tag{5}$$

The climate sensitivities of glacierised and non-glacierised parts (Eqs. (4) and (5)) and the corresponding uncertainties were estimated in the same way as above using the anomalies $\delta Q^{(g)}$ and $\delta Q^{(r)}$, along with δP and δT.

Given the instantaneous glacier fraction x, the quantities defined for the glacierised and non-glacierised part of the catchments are related to those defined for the whole catch-

ment as,

$$\delta Q = x\delta Q^{(g)} + (1-x)\delta Q^{(r)}, \quad (6)$$

$$s_T = xs_T^{(g)} + (1-x)s_T^{(r)}, \quad (7)$$

$$s_P = xs_P^{(g)} + (1-x)s_P^{(r)}. \quad (8)$$

On the glacierised part, we estimated the mass-balance sensitivities to the corresponding temperature and precipitation forcing over the period of 1980–2018. The sensitivities were computed by linearly regressing the modelled anomalies of the mass-balance to those of the annual precipitation and summer air-temperature. The precipitation sensitivity of glacier mass balance was defined to be the mass-balance change due to a 10% change in precipitation following the convention used in the literature (e.g., Wang et al., 2019).

3.3.2 Variability of summer runoff

The climate sensitivities defined above allow determination of the interannual variability of summer runoff given those of P and T,

$$\sigma_Q = \sqrt{s_T^2\sigma_T^2 + s_P^2\sigma_P^2}, \quad (9)$$

where σ_Q, σ_P, and σ_T are standard deviations of Q, P, and T, respectively. An implicit assumption here is that δP and δT are uncorrelated over the simulation period, which we verified to be true at $p < 0.05$ level for both the catchments.

We computed σ_P and σ_T during 1980–1996 and 1997–2018 from the forcing data, and used Eq. (9) to predict the corresponding σ_Q. These predictions were validated using the corresponding σ_Q obtained directly from the simulated summer runoff time series. We analysed the future changes in σ_Q in the studied catchments due to shrinking glaciers, and the variation of σ_Q for a set of hypothetical catchments having different x. Note that an empirical non-monotonic dependence of the coefficient of variation of runoff across catchments on the corresponding fractional glacier cover with a minimum at a moderate glacier cover has been termed as 'glacier-compensation effect' (Chen and Ohmura, 1990).

3.3.3 Long-term changes in mean summer runoff

The climate sensitivities defined above can be used to predict the multidecadal changes in summer runoff (ΔQ) for given changes in annual precipitation (ΔP) and mean summer temperature (ΔT). For a change in glacier fraction Δx from the initial value of x_0 (i.e., $x \doteq x_0 + \Delta x$), the following linear-response equation can be constructed ignoring the terms that were higher order in Δ.

$$\Delta Q = x(s_P^{(g)}\Delta P + s_T^{(g)}\Delta T) + (1-x)(s_P^{(r)}\Delta P + s_T^{(r)}\Delta T) + \Delta x(Q_0^{(g)} - Q_0^{(r)}). \quad (10)$$

A similar linear-response approach was used to analyse glacier-compensation effect (Chen and Ohmura, 1990) without explicitly referring to climate sensitivity. As ERA5 annual precipitation showed low/little spatial variability within the two catchments (supplementary Fig. S4), here we ignored the spatial variation of the generated runoff within the off-glacier or glacierised areas. We also assumed that the contribution of the deglacierised area to the changes in summer runoff is well represented by the difference between the mean runoff of the glacierised and non-glacierised parts. Note that climate-sensitivity based predictions for future changes in runoff are reliable as long as the predicted changes lie within the range of the recent interannual variability of P, T and Q. Beyond this range, there may be uncontrolled extrapolation errors.

Equation (10) was used to investigate the multi-decadal changes in the summer runoff, assuming glacier-loss scenarios in Chandra and upper Dudhkoshi catchments to be the same as those projected for Indus and Ganga basin under RCP 2.6 climate scenario (Huss and Hock, 2018). The corresponding temperature projections were obtained from available estimates for the western and eastern Himalaya, respectively (supplementary Fig.S8 of Kraaijenbrink et al. (2017)). The related precipitation changes, which were not significant within the uncertainties for both the regions (Kraaijenbrink et al., 2017), were ignored here. Consequently, the terms with ΔP in Eq. (10) did not contribute to the estimated changes.

Under a sustained warming, glacier runoff is expected to show a peak over a multidecadal scale due to the excess meltwater contribution from the shrinking glacier reserve, which is followed by a decline in the runoff as the ice reserve depletes (Huss and Hock, 2018). Following (Huss and Hock, 2018), we defined 'peak water' as the maximum change in runoff of the area that was glacierised at 2000 AD, and used Eq. (10) to predict the timing and the magnitude of the 'peak water' in the studied catchments. While the glacier boundaries (Arendt et al., 2017) belonged to 2002, the small changes in glacier area between 2000 and 2002 was ignored for this calculation due to an observed slow rate of glacier area change (Table 1).

4 Results and discussions

4.1 Calibration and validation

The Bayesian calibration method fitted the observed glacier mass balance and the summer runoff data simultaneously, that yield unique best-fit models for both the catchments (Figs. 4a–4b) yielding a unique best-fit model with a optimum pair of DDf and α_P. This is in contrast with the case where using only discharge data for calibration lead to a family of best-fit models (e.g., Azam and Srivastava, 2020). The most-probable DDF values were 5.0 and 7.5 mm day^{-1} $^{\circ}$C^{-1} for Chandra and upper Dudhkoshi catchments, respectively. These DDF values were in the same ballpark range as previously used in studies in and around Chandra (Azam

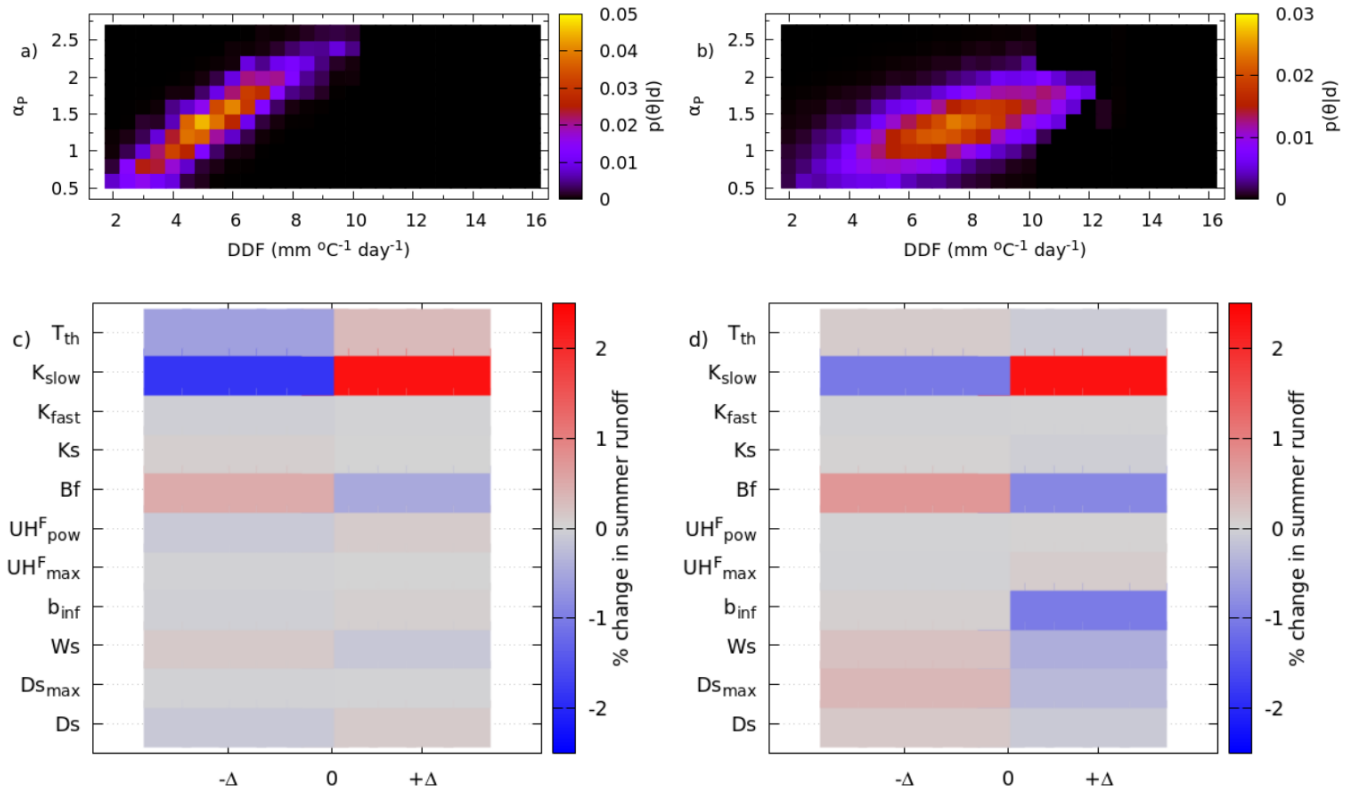

Figure 4. (a) and (b) shows the posterior probability distribution $p(\theta|d)$ of the model parameters (α_P, DDF) for Chandra and upper Dushkoshi catchment, respectively (see Sect. 3.2.3 and 4.1). (c) and (d) shows the sensitivities of the simulated summer runoff to perturbations in 11 uncalibrated model parameters for Chandra and upper Dushkoshi catchments, respectively. Here, $\pm\Delta$ denotes the perturbation of parameters by $\pm 25\%$ of the corresponding prescribed range (see Sect. 3.2.4, and supplementary Table S2).

et al., 2019; Pratap et al., 2019) and Dudhkoshi catchments (Pokhrel et al., 2014; Khadka et al., 2014; Nepal, 2016). The best-fit α_P was 1.4 for both the catchments which was within the range of values 0.7–1.5 used in the existing studies in the Himalaya to correct various reanalysis products (Huss and Hock, 2015; Bhattacharya et al., 2019; Azam and Srivastava, 2020).

The calibrated models reproduced the observed summer runoff of the catchments reasonably well (Fig. 5) with RMSEs of 11 and 12% of the mean summer runoff, and NSEs of 0.88 and 0.80 for Chandra and upper Dudhkoshi catchments, respectively. These RMSE and NSE values were comparable to or smaller than those reported in the existing studies from the region (Nepal, 2016; Mimeau et al., 2018; Bhattacharya et al., 2019; Azam et al., 2019; Azam and Srivastava, 2020). Four additional calibration experiments for upper Dudhkoshi catchment, each one using a different set of 4 consecutive years of runoff data for calibration, obtained most-probable models with DDF (7.2 ± 1.5 mm day^{-1} °C^{-1}), α_P (1.43 ± 0.06), NSEs (0.79–0.86), and RMSEs (10–14% of mean summer runoff) similar to those mentioned above.

To test the statistical significance of the above fits, we computed the probability of having RMSEs of runoff and mass balance equal to or smaller than those in the best-fit model, when the entire model space is sampled uniformly (supplementary Fig. S7). For both discharge and glacier mass balance, these probabilities were 0.03 or smaller in both the catchments, indicating that the fits were significant at $p < 0.05$ level.

4.2 Simulated runoff and its parameter sensitivity

The simulated mean summer runoff of Chandra and upper Dudhkoshi catchments over the period 1980–2018 were 1.08 ± 0.08 and 0.81 ± 0.07 m yr^{-1}, respectively (supplementary Fig. S6). The corresponding standard deviations were 0.14 and 0.10 m yr^{-1}. The mean summer runoff of the glacierised and the non-glacierised parts of Chandra catchment were 1.54 and 0.92 m yr^{-1}, respectively. The corresponding values for upper Dudhkoshi catchment were 1.59 and 0.61 m yr^{-1}. In these two catchments, more than 81% of the simulated annual runoff were during the summer season. In comparison, seven years of observation from upper Dudhkoshi catchment (Chevallier et al., 2017) showed a mean specific summer runoff of 0.86 ± 0.05 m yr^{-1}, which

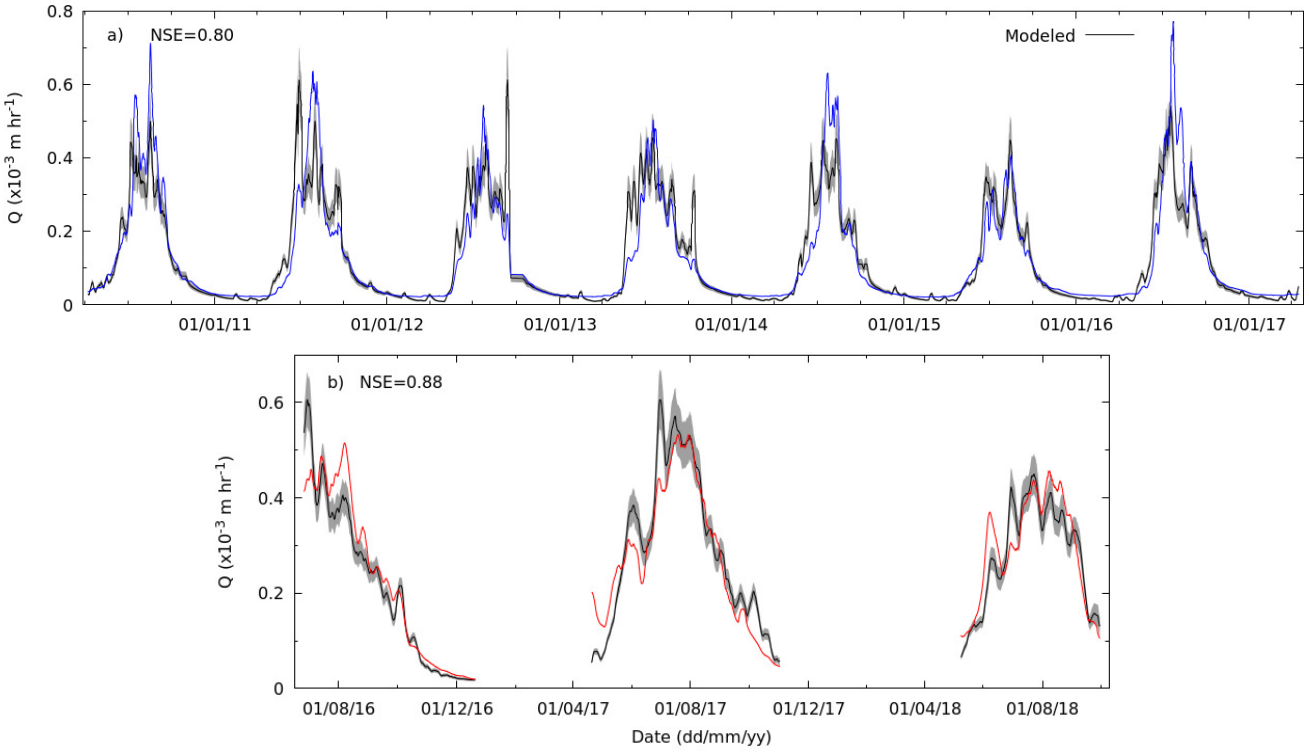

Figure 5. Modelled weekly runoff (black lines, with grey bands denoting 2-σ uncertainty) compared with the corresponding observations for (a) upper Dudhkoshi (blue solid line), and (b) Chandra (red solid line) catchments.

was 83% of the mean annual runoff. Our simulations indicated that glacier runoff contributed 31±12% and 36±16% of the total summer runoff in upper Dudhkoshi and Chandra catchments, with the glacier ice loss amounting to 9% and 4% of the respective total summer runoff (supplementary Fig. S6).

Existing model studies reported annual runoff of 1.6 m yr^{-1} during 2000–2010 (Nepal, 2016) and 0.96 m yr^{-1} during 1981–2015 (Chandel and Ghosh, 2021) for the whole Dudhkoshi catchment (Fig. 2b), and 0.95 m yr^{-1} during 2013–2015 (Mimeau et al., 2018) for Periche sub-catchment (Fig. 2b). The last two estimates compared well to those presented above. Existing estimates (Chandel and Ghosh, 2021) of summer runoff (0.87 m yr^{-1}) and glacier runoff (0.76 m yr^{-1}) of Dudhkoshi catchment were also consistent with our results. No such previous runoff estimates were available for Chandra catchment. The estimated glacier contributions to runoff obtained here were largely consistent with the existing model studies from the region (Nepal, 2016; Engelhardt et al., 2017; Mimeau et al., 2018; Azam et al., 2019; Chandel and Ghosh, 2021) when the differences in fractional glacier cover were taken into account (supplementary Table S4).

The parameter-sensitivity analysis revealed that the absolute changes in summer runoff were less than $\sim 1.5\%$ for all the parameters, except Bf and K_{slow} (Figs. 4b–4d). Slightly higher summer-runoff sensitivities (1.8–2.5 %) for the two longer time scales Bf and K_{slow} became less than 1%, when the annual runoff was considered. The additional 78 simulations where two parameters were perturbed simultaneously, obtained runoff changes almost equal to the sum of those obtained in the corresponding pair of simulations with a single perturbed parameter (supplementary Fig. S5). A generally low parameter sensitivity of the summer runoff implied that the present summer runoff estimates were relatively robust to the uncertainties in 11 uncalibrated glacio-hydrological model parameters (supplementary Table S2).

4.3 Simulated glacier mass balance and its climate sensitivity

The simulated glacier mass balance for Chandra and upper Dudhkoshi catchments over 1980–2018 were -0.18 ± 0.14 and -0.37 ± 0.09 m w.e. yr^{-1}. These estimates were comparable to the existing geodetic observations within the uncertainties (Fig. 6c; supplementary Table S3). The RMSE between modelled and observed mass balance of Chandra and upper Dudhkoshi catchments were 0.10 and 0.11 m w.e. yr^{-1}, respectively.

The sensitivity of the modelled glacier mass balance to temperature was -0.47 ± 0.14 and -0.27 ± 0.10 m yr^{-1} °C^{-1} for Chandra and upper Dudhkoshi catchments, respectively. The corresponding precipitation sensitivities for these

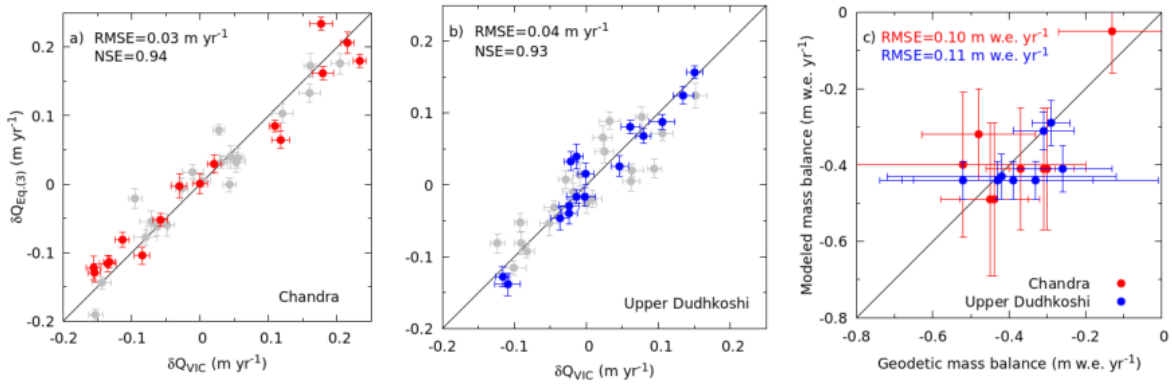

Figure 6. The summer runoff anomalies $\delta Q_{\text{Eq.(3)}}$ as computed using the Eq. (3) are compared with those from the VIC model simulations δQ_{VIC}, for (a) Chandra, and (b) upper Dudhkoshi catchments. The red (blue) solid circles are for Chandra (upper Dudhkoshi) catchment during the validation period 1980–1996. The gray solid circles denote data from the calibration period 1997–2018. (c) A comparison of the modelled glacier mass balance with the available regional-scale geodetic mass balance for Chandra (solid red circles) and upper Dudhkoshi (solid blue circles) catchments. The modeled values are over to the same period as that of the corresponding observed geodetic mass balance (supplementary Table S3). The solid gray line in each plot shows the 1:1 reference line.

catchments were 0.2 ± 0.09 and 0.05 ± 0.05 m yr^{-1} for a 10% change in precipitation. These sensitivities were significant at $p < 0.01$ level. The previously reported mass-balance sensitivities at a regional scale (Shea and Immerzeel, 2016; Sakai and Fujita, 2017; Tawde et al., 2017; Wang et al., 2019) and for individual glaciers from the western and central Himalaya (Azam et al., 2014; Wang et al., 2019; Sunako et al., 2019; Azam and Srivastava, 2020) spanned a wide range (supplementary Table S8). This possibly reflected the corresponding differences of the climate setting, geometry, and topography of the glaciers studied, along with underlying model assumptions, model calibration, input data sets, and so on. The mass-balance sensitivities obtained in the present study were well within the above range. A relatively higher summer temperature sensitivity of the glaciers Chandra catchment compared to those of upper-Dudhkoshi was in apparent contradiction with an expected stronger influence of temperature forcing on summer-accumulation type glaciers due to a conversion between snow and rain (Fujita, 2008; Kumar et al., 2019). However, apart from the precipitation seasonality, mass-balance sensitivity also depends on factors like glacier hypsometry such that a relatively weaker temperature-sensitivity of glaciers in summer-monsoon fed Dudhkoshi compared to that in winter-snow fed Chandra cannot be ruled out. In fact, a similar trend of mass-balance sensitivities over these two regions were also found in a regional-scale energy-balance model study (Sakai and Fujita, 2017).

4.4 Climate sensitivities of catchment runoff

A linear fit of the summer runoff anomalies to those of summer temperature and annual precipitation (Eq. (3)) during 1997–2018 worked well for both Chandra (R^2=0.92) and upper Dudhkoshi (R^2=0.93) catchments. These fits obtained respective temperature sensitivities of summer runoff s_T of 0.12±0.06 and 0.12±0.09 m yr^{-1} °C^{-1} for Chandra and upper Dudhkoshi catchments, respectively. The corresponding best-fit s_P were 0.39±0.07 and 0.47±0.13 m yr^{-1} m^{-1}. These sensitivities were all significant at $p < 0.01$ level. The estimated sensitivities for the two catchments were the same within the limits of uncertainty, and the corresponding percentage changes in runoff were also similar (supplementary Table S5). This may be a surprising feature given the contrasting precipitation regimes of the catchments. This issue is discussed later in the text.

The sensitivities computed over the calibration period (1997–2018) reproduced the variability of summer runoff over the validation period (1980–1996) reasonably well (Figs. 6a–6b) with RMSE < 0.04 m yr^{-1} and NSE > 0.93. This also validated the use of Eq. (3) to predict the interannual variability of summer runoff in these two catchments. The reported temperature sensitivities of summer runoff over the Himalaya were in the range between 5 to 27 % of summer runoff change per °C warming, and the precipitation sensitivities of summer runoff were between -0.6 to 16 % of summer runoff due to 10% changes in P (Fujita and Sakai, 2014; Pokhrel et al., 2014; Azam and Srivastava, 2020) (supplementary Table S6). The previously reported temperature and precipitation sensitivities of summer runoff outside the Himalaya were in the range between 9 to 24 % of summer runoff per °C warming, and 2 to 7 % of summer runoff due to 10% changes in P (Engelhardt et al., 2015; He, 2021), respectively. The temperature and precipitation sensitivities of summer runoff obtained in the present study, 11–14 % of summer runoff per °C warming and 6–9 % of summer runoff due to 10% changes in P, respectively, were with the

above range. It appears that the differences in climate sensitivities of runoff obtained in different studies are mostly due to the corresponding differences in glacier fraction of the catchments studied, as there is a monotonic variation of the sensitivities with glacier fractions (supplementary Table S6).

During 1980–2018, the simulated summer runoff in Chandra and upper Dudhkoshi catchments varied in the range 0.86–1.33 and 0.55–0.98 m yr^{-1}, respectively. The respective ranges of summer temperature were 2.0–5.3 and 1.2–2.3°C, and those of annual precipitation were 1.05–2.10 and 1.17–1.92 m yr^{-1}. As discussed before, the sensitivities estimated above are applicable within the above range of precipitation and temperature forcing. Note that in both the catchments, s_P was significantly smaller than 1 m yr^{-1} m^{-1}. This indicated an interannual change of the storage in the glaciers, and a change in evapotranspiration from the off-glacier area in response to the precipitation forcing (see Sects. 4.5 and 4.6).

4.5 Climate sensitivities of glacier runoff

The estimated temperature sensitivities of glacier runoff $s_T^{(g)}$ were 0.41±0.08 and 0.47±0.11 m yr^{-1} °C^{-1} for Chandra and upper Dudhkoshi catchments, respectively (significant at $p < 0.01$ level). The corresponding precipitation sensitivities $s_P^{(g)}$ were −0.12±0.14 and 0.00±0.07 m yr^{-1} m^{-1} (not significant at $p < 0.05$ level). A compilation of glacier runoff sensitivities (supplementary Table S7) indicated that the sensitivities reported by here were largely in line with those reported previously in the Himalaya (Fujita and Sakai, 2014; Chandel and Ghosh, 2021) and elsewhere (Anderson et al., 2010; Soruco et al., 2015; Pramanik et al., 2018). Again, both the catchments had similar absolute values of $s_P^{(g)}$ and $s_T^{(g)}$ within the corresponding uncertainties. The corresponding percentage sensitivity values were also similar, except a somewhat higher percentage change in glacier runoff due to unit temperature change in upper Dudhkoshi catchment (supplementary Table S5).

Interestingly, summer runoff of both winter-accumulation type glaciers in Chandra catchment and summer-accumulation type glaciers in upper Dudhkoshi catchment was approximately independent of the corresponding precipitation variabilities. This confirmed the general result, which was derived previously using a simple temperature-index model (Banerjee, 2022), that irrespective of the glacier chosen, the climate setting, or the model used, glacier runoff has a weak to no precipitation sensitivity.

In both the studied catchments, a positive precipitation anomaly did not translate into a higher summer runoff of the glaciers (Fig. 7). With increasing precipitation, the rainfall on glacier did not change, and snowmelt showed a very weak (Chandra) to no (upper Dudhkoshi) increase (Fig. 7). This implied that a higher precipitation contributed mostly to a positive storage change (snow accumulation) on the glaciers. In addition, a higher snowcover and/or an association between higher-than-normal precipitation and lower mean temperature (not statistically significant) caused a decline in glacier melt, and amplified the changes in glacier storage change (Fig. 7). These effects combined to yield a nearly precipitation-insensitive glacier runoff in both the catchments. In contrast, a higher glacier melt with increasing mean summer temperature caused a relatively high temperature sensitivity of $Q^{(g)}$ in both the catchments (Fig. 7). Here, the glaciers effectively acted as infinite reservoirs over an annual scale so that the meltwater volume was limited only by the available energy. A higher temperature implied a higher available energy, and thus a higher meltwater flux from the glaciers. These arguments were consistent with a high correlation ($r > 0.9, p < 0.05$) between the summer temperature and summer runoff of the glacierised parts for both the catchments (Fig. 7).

The negligible $s_P^{(g)}$ discussed above implied a stabilisation of the total runoff of the glacierised catchments against precipitation variability (e.g. Van Tiel et al., 2021), as the runoff contribution from the glacierised fraction x was essentially independent of precipitation (Eq. 8). The magnitude of the precipitation sensitivity of catchment runoff s_P is thus expected to decrease with the glacier fraction x. This stabilising effect (Banerjee, 2022) is consistent with a reported buffering of catchment runoff by glaciers during the extreme drought years across High Mountain Asia (Pritchard, 2019).

4.6 Climate sensitivity of runoff of the non-glacierised parts

In the non-glacierised parts of Chandra and upper Dudhkoshi catchments, $s_T^{(r)}$ of 0.02±0.06 and 0.03±0.10 m yr^{-1} °C^{-1} and $s_P^{(r)}$ of 0.56±0.10 and 0.59±0.12 m yr^{-1} m^{-1} were obtained, respectively. These sensitivities were all significant at $p < 0.01$ level. Again, both the catchments had similar absolute values of $s_P^{(r)}$ and $s_T^{(r)}$ within the corresponding uncertainties, and the corresponding percentage sensitivity values were similar (supplementary Table S5).

Compared to the sensitivities of glacier runoff, the climate sensitivities of the runoff from the non-glacierised parts showed an exactly opposite trend. The summer runoff of the off-glacier areas were relatively insensitive to temperature anomalies, but sensitive to precipitation anomalies (supplementary Fig. S8). Because of the presence of seasonal snow cover over the non-glacierised parts, a temperature dependence of the summer runoff may be expected. However, the total amount of snowmelt during the summer was limited by the supply of seasonal snow, and not by the available energy. This led to a weak response of the total summer runoff from the non-glacierised parts to temperature forcing. This argument was supported by the fact that the summer runoff from the non-glacierised parts were uncorrelated with summer

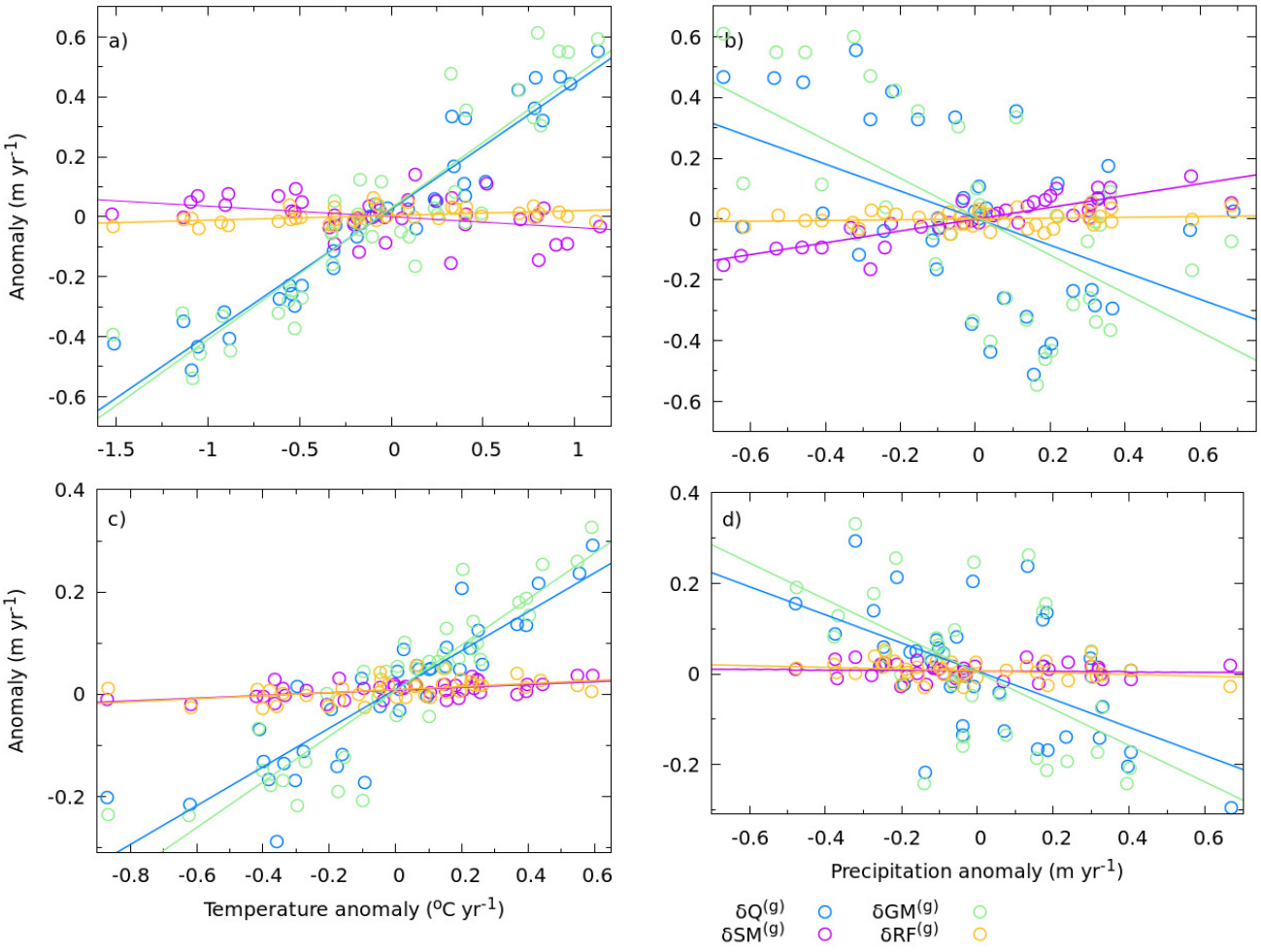

Figure 7. The anomalies of glacier runoff $\delta Q^{(g)}$, and its components, namely, snowmelt $\delta SM^{(g)}$, glacier ice melt $\delta GM^{(g)}$, and rainfall $\delta RF^{(g)}$ for the glacierised parts of the catchments are plotted as a unction of the corresponding temperature and precipitation anomalies: (a, b) for Chandra catchment, and (c, d) for upper Dudhkoshi catchment. The corresponding best-fit straight lines are also shown.

temperature and strongly correlated with summer precipitation ($r > 0.9, p < 0.05$). Our results suggest that the precipitation changes in these two catchments caused comparable changes in surface runoff, groundwater/baseflow, and evapotranspiration (Supplementary Fig. S8). Consequently, about ∼2/3rd of the precipitation anomaly translated to that of the total runoff. Interestingly, evapotranspiration anomalies in the glacier-free parts of Chandra (upper Dudhkoshi) were controlled by the summer temperature (precipitation) (Supplementary Fig. S8). This suggested a water-limited condition in the summer monsoon-fed upper Dudhkoshi catchment, and an energy-limited condition in the winter snow-fed Chandra catchment.

4.7 Implications of the estimated climate sensitivities

The above estimated climate sensitivities from glacierised and non-glacierised parts of the catchments suggested $s_P^{(g)} \approx 0$ and $s_T^{(r)} \approx 0$. Thus, Eqs. (3)–(10) can be simplified to the following approximate relations describing the response of the summer runoff to climate variability and change in these two catchments.

$$\delta Q \approx x s_T^{(g)} \delta T + (1-x) s_P^{(r)} \delta P, \quad (11)$$

$$\delta Q^{(g)} \approx x s_T^{(g)} \delta T, \quad (12)$$

$$\delta Q^{(r)} \approx (1-x) s_P^{(r)} \delta P, \quad (13)$$

$$\sigma_Q \approx \sqrt{x^2 s_T^{(g)2} \sigma_T^2 + (1-x)^2 s_P^{(r)2} \sigma_P^2}, \quad (14)$$

$$\Delta Q \approx x s_T^{(g)} \Delta T + (1-x) s_P^{(r)} \Delta P + \Delta x (Q_0^{(g)} - Q_0^{(r)}) \quad (15)$$

These simplified equation suggested that the key parameters that determined the climate response of these glacierised catchments to given climate forcing were $s_T^{(g)}$ and $s_P^{(r)}$. According to Eq. (11), the precipitation and temperature sensitivity of catchment runoff are essentially given by $(1-x)s_P^{(r)}$

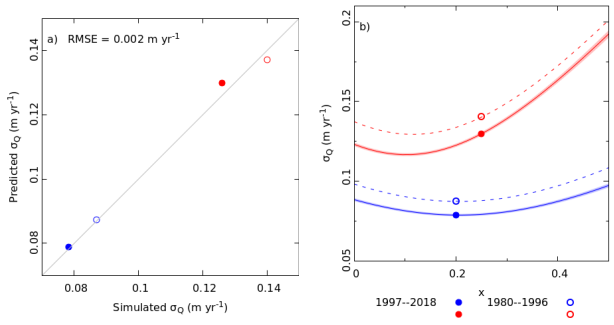

Figure 8. a) Predicted σ_Q using Eq. (14) are compared with the corresponding simulated values for both the catchments. The solid and open circles denote data for the periods 1997–2018 and 1980–1996, respectively. Data for Chandra and upper Dudhkoshi catchments are shown with red and blue symbols, respectively. b) The solid (dashed) lines show $\sigma_Q(x)$ obtained using σ_T and σ_T values from 1997–2018 (1980–1996).

and $xs_T^{(g)}$, respectively. As both the catchments had similar $s_P^{(r)}$, the corresponding s_P were also similar with a slightly smaller value in Chandra catchment due to a higher fractional glacier cover there. On the other hand, a slightly higher $s_T^{(g)}$ in upper Dudhkoshi catchment, together with a slightly lower glacier cover there, led to similar s_T in the two catchments. Below we discuss the implications of the above simplified linear-response formulae for the future changes in the mean summer runoff and its variability.

4.7.1 Summer runoff variability

Over the calibration period 1997–2018, Chandra and upper Dudhkoshi catchments had σ_P of 0.22 and 0.15 m yr^{-1}, and σ_T of 0.89 and 0.34 °C, respectively. These values, together Eq. (14), predicted σ_Q of 0.13 and 0.08 m yr^{-1} for the two catchments, which equalled the corresponding values obtained directly from the simulated summer runoff (Fig. 8a). A corresponding close match was also obtained over the validation period of 1980-1996 (Fig. 8a).

Equation (14)) can also be used to predict the variation of $\sigma_Q$in these catchments due to the shrinkage glacier cover if σ_P and σ_T were to remain unchanged. The shape of hyperbolic $\sigma_Q(x)$ curve for both the catchments (Fig. 8b) indicated that major changes in runoff variability may not take place due to the expected glacier loss alone. However, possible changes in σ_P and σ_T may drive significant future changes of σ_Q in these two catchments, as underlined by the difference between the simulated σ_Q for the two catchments over the periods 1980–1996 and 1997–2018 (Fig. 8b).

4.7.2 Glacier-compensation curve

For a set of hypothetical catchments with different values of x, but similar $s_T^{(g)}$, $s_P^{(r)}$, σ_T and σ_P, Eq. (14) implies that σ_Q is a hyperbolic function of x (Fig. 8b). The runoff variability is high in the limit $x \to 0$ due to a precipitation sensitive off-glacier runoff with $\sigma_Q \approx (1-x)s_P^{(r)}\sigma_P$. In the opposite limit of $x \to 1$, σ_Q is again high due to a high temperature sensitivity of glacier runoff, with $\sigma_Q \approx xs_T^{(g)}\sigma_T$. These two competing effects yield a minimum in σ_Q at an intermediate value of x (Fig. 8b) (Banerjee, 2022). This nonmonotonic behaviour of runoff variability with x is well known empirically (e.g., Chen and Ohmura, 1990), and is termed as glacier-compensation effect. The above theoretical explanation of the effect is consistent with a reported strong correlation between runoff and precipitation (temperature) in the limit of small (extensive) glacier cover (Van Tiel et al., 2020a). Note that while Eq. (14) suggests a hyperbolic glacier compensation curve, some of the existing studies used an empirical parabolic curve (e.g., Chen and Ohmura, 1990). As glacier cover shrink, the summer runoff from both the studied catchments is expected to become more sensitive to precipitation forcing (Eq. (14)).

Chen and Ohmura (1990) suggested that the glacier-compensation curve can be utilised to estimate the change in σ_Q as glacier cover changes. However, recent model simulations indicated that a time-dependent glacier-compensation curve rules out such possibility (Van Tiel et al., 2020a). This is consistent with Eq. (14), which indicates that apart from a changing glacier cover, the compensation curve (and thus σ_Q) can shift when σ_P and/or σ_T changes with time.

4.7.3 Changes in mean summer runoff and prediction of peak water

As discussed before, estimating the future changes mean summer runoff using Eq. (15) requires the changes in summer precipitation or temperature to be within the range of calibration (Sect. 3.2.3). Only for Chandra catchment, the optimistic RCP 2.6 scenario (supplementary Fig. S9), temperature change by ∼2050 was within the range of annual temperature over the period 1980–2018 and the present estimates of climate sensitivities could be used safely. The projected mean temperature changes of 1.1°C by 2050 under RCP 2.6 scenario were within the calibration range, and obtained a glacier runoff change of 0.27±0.03 m yr^{-1} (assuming $x_0 = 1$ at 2000). This was comparable to the corresponding reported estimate of 0.25 m yr^{-1} for the entire Indus basin (Huss and Hock, 2018).

The predicted future changes of glacier runoff in Chandra catchments, using Eq. (15), reproduced the peak-water effect successfully (Fig. 9). The estimated peak water was 12±8% of the present glacier runoff, and the estimated timing was 2033±7. In Chandra catchment, the estimated peak-water in glacier runoff is expected to cause a 0.05 m yr^{-1} to rise in catchment runoff. This change may not be detectable, given the recent interannual variability of catchment runoff $\sigma_Q = 0.14$ m yr^{-1}. Note that the above estimates are comparable to previously predicted a peak water of 14±3% on

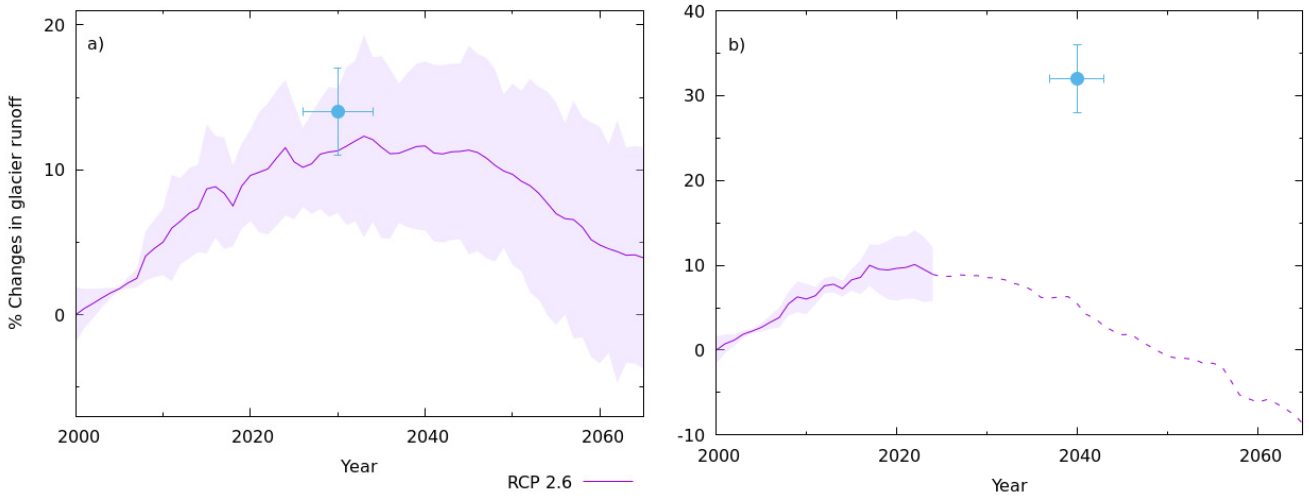

Figure 9. The 'peak water' due to future glacier changes predicted using Eq. (15) for (a) Chandra, and (b) upper Dudhkoshi catchments, respectively. The solid sky-blue dots represents the corresponding 'peak water' as reported in Huss and Hock (2018) for both the catchments. Dashed portion of the solid line in upper Dudhkoshi catchment indicate the corresponding temperature change beyond the calibration range of the catchment. See text for details.

2030±4 (Huss and Hock, 2018). It is encouraging that a simple climate-sensitivity based approach presented here could capture the peak-water effect in Chandra catchment as well as a state-of-the-art glacio-hydrological model (Huss and Hock, 2018). Note that for Chandra catchment, our simulated recent glacier runoff, the initial glacier cover, and geodetic mass balance used for calibration were similar to the corresponding values used by Huss and Hock (2018) for the Indus basin.

In upper Dudhkoshi catchment, we estimated a peak water of 10±4% of the present glacier runoff, and the estimated timing was 2022±4 (Fig). This estimated peak water was significantly smaller and quicker compared to that of Huss and Hock (2018). This inconsistency may be related to possible extrapolation errors as, the projected temperature changes crossed the range of interannual variability by 2024. Moreover, there were several difference between the two models in this region, which may contribute to the above mismatch. The RGI 4 glacier inventory used by Huss and Hock (2018) had 25% higher glacier cover in Ganga basin compared to RGI 6 used here. Also the authors calibrated their model using a geodetic mass-balance record which was twice as negative as the median of the eight geodetic mass balance records used here. Also, the present estimates of glacier runoff in upper Dudhkoshi catchment was almost half of that reported by Huss and Hock (2018) for Ganga basin. The above differences likely led to a corresponding large difference in the modelled climate sensitivities of glacier runoff between the present study and that of Huss and Hock (2018) in this region.

5 Summary and conclusions

In this paper, we simulate the summer runoff of Chandra (western Himalaya) and upper Dudhkoshi (eastern Himalaya) catchments over 1980–2018, using the VIC model augmented with a temperature-index glacier-melt module. Calibrating two model parameters using a Bayesian method that simultaneously fits the available summer runoff and decadal-scale geodetic glacier mass balance, our simulation obtained a statistically significant fit to the available observations. The interannual variability of the simulated summer runoff is then utilised to obtain the climate sensitivity of summer runoff to summer temperature and annual precipitation forcing. Despite their contrasting climate regimes, the eastern and the western Himalayan catchments show similar climate sensitivities of the total summer runoff, and that generated from glacerised and nonglacerised parts of the catchments. The simulated climate sensitivities of summer runoff to temperature and precipitation forcing in the catchments reveal interesting patterns: the precipitation sensitivities of the summer runoff of the non-glacierised parts of the catchments are high, but those of the glacierised parts are negligible. In contrast, the temperature sensitivities of summer runoff of glaciers are high, but those of the non-glacierised parts are negligible. The estimated climate sensitivities of summer runoff are also used to obtain analytical insights into several well known characteristics of the climate response of runoff from glacierised catchments, including the buffering effect, glacier-compensation effect, and the peak water effect. For the two Himalayan catchments, our approximate analysis suggests that the impacts of the future glacier loss on the long-term mean and variability of catchment runoff

may not be detectable, given the relatively large interannual runoff variability in these catchments. However, with a depleting glacier cover, the variability of summer runoff in these two catchments is likely to become more sensitive to precipitation variability. Despite the limitations like the simplifying model assumptions, and the calibration with a limited dataset, the present study brings out the usefulness of a climate-sensitivity based approach to understand and predict the future changes in runoff of glacierised catchments in the Himalaya.

Data availability. The VIC model can be downloaded from https://vic.readthedocs.io/en/master/. The additional codes developed here for glacier melt modelling and routing can be accessed at https://osf.io/7une2/. All the hydro-meteorological observations used here for upper Dudhkoshi and Chandra catchments are available from http://www.papredata.org/ and Head, Himalayan Cryosphere studies, NCPOR (email: hcryo@ncpor.res.in) upon request.

Author contributions. AB conceived the study, and developed the theoretical framework. SL ran the simulations. SL and AB did the data analysis. AB wrote the manuscript with inputs from SL. AS, PS, and MT did the field measurements at Chandra catchment, and analysed the field data. All the authors participated in the discussions, and edited the manuscript.

Competing interests. The authors have no competing interests to declare.

Acknowledgements. The study is funded under the HiCOM initiative by ESSO-NCPOR, MoES (grant number NCAOR/2018/HiCOM/04). SL acknowledges INSPIRE Research fellowship (grant no IF 170526). AB acknowledges support from MoES grant no MoES/PAMC/H&C/79/2016-PC-II. We thank the French Agence Nationale de la Recherche (references ANR-09-CEP-0005-04/PAPRIKA and ANR-13-SENV-0005-03/PRESHINE) for sharing the hydro-meteorological data in the upper Dushkoshi catchment. We greatly benefited from discussions with Subimal Ghosh, Pradeep P Mujumdar, and Raghu Murtugudde. Vikram Chandel, Ela Chawla, Arijeet Dutta, and Sneha Potghan helped with VIC model setup and input data.

References

Anderson, B., Mackintosh, A., Stumm, D., George, L., Kerr, T., Winter-Billington, A., and Fitzsimons, S. Climate sensitivity of a high-precipitation glacier in New Zealand, Journal of Glaciology, 56(195), 114-128, 10.3189/002214310791190929, 2010.

Amante, C. and B.W. Eakins.: ETOPO1 1 Arc-Minute Global Relief Model: Procedures, Data Sources and Analysis. NOAA Technical Memorandum NESDIS NGDC-24, National Geophysical Data Center, NOAA, 10.7289/V5C8276M, 2009.

Andreadis, K. M., Storck, P., and Lettenmaier, D. P.: Modeling snow accumulation and ablation processes in forested environments, Water resources research, 45(5), 10.1029/2008WR007042, 2009.

Arendt, A., Bliss, A., Bolch, T., Cogley, J. G., Gardner, A., Hagen, J. O., ... and Zheltyhina, N.: Randolph Glacier Inventory–A Dataset of Global Glacier Outlines: Version 6.0: Technical Report, Global Land Ice Measurements from Space, https://doi.org/10.7265/N5-RGI-60, 2017.

Azam, M. F., Wagnon, P., Vincent, C., Ramanathan, A., Linda, A., Singh, V. B.: Reconstruction of the annual mass balance of Chhota Shigri glacier, Western Himalaya, India, since 1969, Annals of Glaciology, 55(66), 69-80, https://doi.org/10.3189/2014AoG66A104, 2014.

Azam, M. F., Wagnon, P., Vincent, C., Ramanathan, A. L., Kumar, N., Srivastava, S., ... Chevallier, P.: Snow and ice melt contributions in a highly glacierized catchment of Chhota Shigri Glacier (India) over the last five decades, Journal of Hydrology, 574, 760-773, https://doi.org/10.1016/j.jhydrol.2019.04.075, 2019.

Azam, M. F., and Srivastava, S.: Mass balance and runoff modelling of partially debris-covered Dokriani Glacier in monsoon-dominated Himalaya using ERA5 data since 1979, Journal of Hydrology, 125432, https://doi.org/10.1016/j.jhydrol.2020.125432, 2020.

Azam, M. F., Kargel, J. S., Shea, J. M., Nepal, S., Haritashya, U. K., Srivastava, S., ... and Bahuguna, I. M.: Glaciohydrology of the Himalaya-Karakoram, Science, 10.1126/science.abf3668, 2021.

Banerjee, A., Patil, D., and Jadhav, A.: Possible biases in scaling-based estimates of glacier change: a case study in the Himalaya, The Cryosphere, 14(9), 3235-3247, https://doi.org/10.5194/tc-14-3235-2020, 2020.

Banerjee, A.: A weak precipitation sensitivity of glacier runoff, Geophysical Research Letters, 49(5), e2021GL096989, 10.1029/2021GL096989, 2022.

Beven, K., Freer, J.: Equifinality, data assimilation, and uncertainty estimation in mechanistic modelling of complex environmental systems using the GLUE methodology, J. Hydrol. 249 (1–4), 11–29, https://doi.org/10.1016/S0022-1694(01) 00421-8, 2001.

Bhattacharya, T., Khare, D., and Arora, M.: A case study for the assessment of the suitability of gridded reanalysis weather data for hydrological simulation in Beas river basin of North Western Himalaya, Applied Water Science, 9(4), 110, https://doi.org/10.1007/s13201-019-0993-x, 2019.

Bolch, T., Pieczonka, T., and Benn, D. I.: Multi-decadal mass loss of glaciers in the Everest area (Nepal Himalaya) derived from stereo imagery, The Cryosphere, 5(2), 349-358, https://doi.org/10.5194/tc-5-349-2011, 2011.

Brun, F., Berthier, E., Wagnon, P., Kaab, A., Treichler, D.: A spatially resolved estimate of High Mountain Asia glacier mass balances from 2000 to 2016, Nature geoscience, 10(9), 668-673, https://doi.org/10.1038/ngeo2999, 2017.

Chandel, V. S., and Ghosh, S.: Components of Himalayan River Flows in a Changing Climate, Water Resources Research, 57(2), e2020WR027589, https://doi.org/10.1029/2020WR02758, 2021.

Chen, J., and Ohmura, A.: On the influence of Alpine glaciers on runoff, IAHS Publ, 193, 117-125, 1990.

Chevallier, Pierre, François Delclaux, Patrick Wagnon, Luc Neppel, Yves Arnaud, Michel Esteves, Devesh Koirala, Yves Lejeune, Frédéric Hernandez, Rémi Muller, Jean-Philippe Chazarin, Jean-François Boyer, Isabelle Sacareau.: Paprika - Preshine hy-

drology data sets in the Everest Region (Nepal), 2010-18, Data base, https://doi.org/10.23708/000521, 2017.

Dooge, J. C. I., Bruen, M., Parmentier, B.: A simple model for estimating the sensitivity of runoff to long-term changes in precipitation without a change in vegetation, Advances in Water Resources, 23(2), 153-163, https://doi.org/10.1016/S0309-1708(99)00019-6, 1999.

Engelhardt, M., Schuler, T. V., and Andreassen, L. M.: Sensitivities of glacier mass balance and runoff to climate perturbations in Norway, Annals of Glaciology, 56(70), 79-88, 10.3189/2015AoG70A004, 2015.

Engelhardt, M., Ramanathan, A. L., Eidhammer, T., Kumar, P., Landgren, O., Mandal, A., and Rasmussen, R.: Modelling 60 years of glacier mass balance and runoff for chhota shigri glacier, western himalaya, northern India, Journal of Glaciology, 63 (240), 618–628. https://doi.org/10.1017/jog.2017.29, 2017.

Farr, T. G., Rosen, P. A., Caro, E., Crippen, R., Duren, R., Hensley, S., ... Seal, D.: The shuttle radar topography mission, Reviews of geophysics, 45(2), https://doi.org/10.1029/2005RG000183, 2007.

Friedl, M., Sulla-Menashe, D.: MCD12Q1 MODIS/Terra+Aqua Land Cover Type Yearly L3 Global 500m SIN Grid V006 [Data set], NASA EOSDIS Land Processes DAAC, Accessed 2020-09-15 from https://doi.org/10.5067/MODIS/MCD12Q1.006, 2019.

Fujita, K.: Effect of precipitation seasonality on climatic sensitivity of glacier mass balance, Earth and Planetary Science Letters, 276(1-2), 14-19, 10.1016/j.epsl.2008.08.028, 2008.

Fujita, K., and Sakai, A.: Modelling runoff from a Himalayan debris-covered glacier, Hydrology and Earth System Sciences, 18(7), 2679-2694. https://doi.org/10.5194/hess-18-2679-2014, 2014.

Gardelle, J., Berthier, E., Arnaud, Y.: Impact of resolution and radar penetration on glacier elevation changes computed from DEM differencing, Journal of Glaciology, 58(208), 419-422, https://doi.org/10.3189/2012JoG11J175, 2012.

Hannah, D. M., and Gurnell, A. M.: A conceptual, linear reservoir runoff model to investigate melt season changes in cirque glacier hydrology, Journal of hydrology, 246(1-4), 123-141, https://doi.org/10.1016/S0022-1694(01)00364-X, 2001.

Herreid, S., and Pellicciotti, F. (2020). The state of rock debris covering Earth's glaciers. Nature Geoscience, 13(9), 621-627, https://doi.org/10.1038/s41561-020-0615-0.

He, Z.: Sensitivities of hydrological processes to climate changes in a Central Asian glacierized basin, Frontiers in Water, 3, 46, https://doi.org/10.3389/frwa.2021.683146, 2021.

Hersbach, H., Bell, B., Berrisford, P., Hirahara, S., Horányi, A., Munoz-Sabater, J., ... Simmons, A.: The ERA5 global reanalysis, Quarterly Journal of the Royal Meteorological Society, 146(730), 1999-2049, https://doi.org/10.1002/qj.3803, 2020.

Hock, R.: Temperature index melt modelling in mountain areas, Journal of hydrology, 282(1-4), 104-115, https://doi.org/10.1016/S0022-1694(03)00257-9, 2003.

Hock, R., Jansson, P., and Braun, L. N.: Modelling the response of mountain glacier discharge to climate warming. In Global change and mountain regions (pp. 243-252), Springer, Dordrecht, https://doi.org/10.1007/1-4020-3508-X_25, 2005.

Huss, M., and Hock, R.: A new model for global glacier change and sea-level rise, Frontiers in Earth Science, 3, 54, https://doi.org/10.3389/feart.2015.00054, 2015.

Huss, M., Hock, R.: Global-scale hydrological response to future glacier mass loss, Nature Climate Change, 8(2), 135-140, https://doi.org/10.1038/s41558-017-0049-x, 2018.

Johnson, E., and Rupper, S.: An examination of physical processes that trigger the albedo-feedback on glacier surfaces and implications for regional glacier mass balance across High Mountain Asia, Frontiers in Earth Science, 8, 129, https://doi.org/10.3389/feart.2020.00129, 2020.

Jost, G., Moore, R. D., Menounos, B., and Wheate, R.: Quantifying the contribution of glacier runoff to streamflow in the upper Columbia River Basin, Canada, Hydrology and Earth System Sciences, 16(3), 849-860, https://doi.org/10.5194/hess-16-849-2012, 2012.

King, O., Quincey, D. J., Carrivick, J. L., and Rowan, A. V.: Spatial variability in mass loss of glaciers in the Everest region, central Himalayas, between 2000 and 2015, The Cryosphere, 11, 407–426, https://doi.org/10.5194/tc-11-407-2017

Koppes, M., Rupper, S., Asay, M., and Winter-Billington, A.: Sensitivity of glacier runoff projections to baseline climate data in the Indus River basin, Frontiers in Earth Science, 3:59, https://doi.org/10.3389/feart.2015.00059, 2015.

Khadka, D., Babel, M. S., Shrestha, S., Tripathi, N. K.: Climate change impact on glacier and snow melt and runoff in Tamakoshi basin in the Hindu Kush Himalayan (HKH) region, Journal of Hydrology, 511, 49-60, https://doi.org/10.1016/j.jhydrol.2014.01.005, 2014.

Kraaijenbrink, P. D. A., Bierkens, M. F. P., Lutz, A. F., Immerzeel, W. W.: Impact of a global temperature rise of 1.5 degrees Celsius on Asias glaciers, Nature, 549(7671), 257-260, https://doi.org/10.1038/nature23878, 2017.

Kumar, P., Saharwardi, M. S., Banerjee, A., Azam, M. F., Dubey, A. K., and Murtugudde, R.: Snowfall variability dictates glacier mass balance variability in Himalaya-Karakoram. Scientific reports, 9(1), 1-9, 10.1038/s41598-019-54553-9, 2019.

Laha, S., Kumari, R., Singh, S., Mishra, A., Sharma, T., Banerjee, A., ... Shankar, R.: Evaluating the contribution of avalanching to the mass balance of Himalayan glaciers, Annals of Glaciology, 58(75pt2), 110-118, https://doi.org/10.1017/aog.2017.27, 2017.

Lang, H.: Forecasting meltwater runoff from snow-covered areas and from glacier basins, In River flow modelling and forecasting (pp. 99-127), Springer, Dordrecht, https://doi.org/10.1007/978-94-009-4536-4_5, 1986.

Liang, X., Wood, E. F., Lettenmaier, D. P.: Surface soil moisture parameterization of the VIC-2L model: Evaluation and modification, Global and Planetary Change, 13(1-4), 195-206, https://doi.org/10.1016/0921-8181(95)00046-1, 1996.

Lohmann, D., Raschke, E., Nijssen, B., Lettenmaier, D. P.: Regional scale hydrology: I. Formulation of the VIC-2L model coupled to a routing model, Hydrological sciences journal, 43(1), 131-141, https://doi.org/10.1080/02626669809492107, 1998.

Maurer, J. M., Schaefer, J. M., Rupper, S., Corley, A.: Acceleration of ice loss across the Himalayas over the past 40 years, Science advances, 5(6), eaav7266, 10.1126/sciadv.aav7266, 2019.

Miles, E. S., Steiner, J. F., Buri, P., Immerzeel, W. W., and Pellicciotti, F. (2022). Controls on the relative melt rates of debris-covered glacier surfaces. Environmental Research Letters, 17(6), 064004, https://doi.org/10.1088/1748-9326/ac6966.

Mimeau, L., Esteves, M., Zin, I., Jacobi, H.-W., Brun, F., Wagnon, P., Koirala, D., and Arnaud, Y.: Quantification of different

flow components in a high-altitude glacierized catchment (Dudh Koshi, Himalaya): some cryospheric-related issues, Hydrol. Earth Syst. Sci., 23, 3969–3996, https://doi.org/10.5194/hess-23-3969-2019, 2019.

Mukherjee, K., Bhattacharya, A., Pieczonka, T., Ghosh, S., Bolch, T.: Glacier mass budget and climate reanalysis data indicate a climatic shift around 2000 in Lahaul-Spiti, western Himalaya, Climatic change, 148(1), 219-233, https://doi.org/10.1007/s10584-018-2185-3, 2018.

Fischer, G., F. Nachtergaele, S. Prieler, H.T. van Velthuizen, L. Verelst, D. Wiberg.: Global Agro-ecological Zones Assessment for Agriculture (GAEZ 2008). IIASA, Laxenburg, Austria and FAO, Rome, Italy, 2008.

Nepal, S.: Impacts of climate change on the hydrological regime of the Koshi river basin in the Himalayan region, Journal of Hydro-Environment Research, 10, 76-89, https://doi.org/10.1016/j.jher.2015.12.001, 2016.

Nie, Y., Pritchard, H. D., Liu, Q., Hennig, T., Wang, W., Wang, X., ... and Chen, X.: Glacial change and hydrological implications in the Himalaya and Karakoram, Nature reviews earth & environment, 2(2), 91-106, https://doi.org/10.1038/s43017-020-00124-w, 2021.

Nuimura, T., Fujita, K., Yamaguchi, S., Sharma, R. R.: Elevation changes of glaciers revealed by multitemporal digital elevation models calibrated by GPS survey in the Khumbu region, Nepal Himalaya, 1992-2008, Journal of Glaciology, 58(210), 648-656, https://doi.org/10.3189/2012JoG11J061, 2012.

Oulkar, S. N., Thamban, M., Sharma, P., Pratap, B., Singh, A. T., Patel, L. K., ... and Ravichandran, M.: Energy fluxes, mass balance, and climate sensitivity of the Sutri Dhaka Glacier in the western Himalaya. Frontiers in Earth Science, 10, 949735, https://doi.org/10.3389/feart.2022.949735, 2022.

Pokhrel, B. K., Chevallier, P., Andreassian, V., Tahir, A. A., Arnaud, Y., Neppel, L., ... Budhathoki, K. P.: Comparison of two snowmelt modelling approaches in the Dudh Koshi basin (eastern Himalayas, Nepal), Hydrological sciences journal, 59(8), 1507-1518, https://doi.org/10.1080/02626667.2013.842282, 2014.

Pratap, B., Sharma, P., Patel, L., Singh, A. T., Gaddam, V. K., Oulkar, S., Thamban, M.: Reconciling High Glacier Surface Melting in Summer with Air Temperature in the Semi-Arid Zone of Western Himalaya, Water, 11(8), 1561, https://doi.org/10.3390/w11081561, 2019.

Pramanik, A., Van Pelt, W., Kohler, J., and Schuler, T. V.: Simulating climatic mass balance, seasonal snow development and associated freshwater runoff in the Kongsfjord basin, Svalbard (1980–2016), Journal of Glaciology, 64(248), 943-956, 10.1017/jog.2018.80, 2018.

Pritchard, H. D.: Asia's shrinking glaciers protect large populations from drought stress, Nature, 569(7758), 649-654, https://doi.org/10.1038/s41586-019-1240-1, 2019.

Rodell, M., P.R. Houser, U. Jambor, J. Gottschalck, K. Mitchell, C.-J. Meng, K. Arsenault, B. Cosgrove, J. Radakovich, M. Bosilovich, J.K. Entin, J.P. Walker, D. Lohmann, and D. Toll.: The Global Land Data Assimilation System, Bull. Amer. Meteor. Soc., 85(3), 381-394, https://doi.org/10.1175/BAMS-85-3-381, 2004.

Rounce, D. R., King, O., McCarthy, M., Shean, D. E., and Salerno, F. (2018). Quantifying debris thickness of debris-covered glaciers in the Everest region of Nepal through inversion of a subdebris melt model. Journal of Geophysical Research: Earth Surface, 123(5), 1094-1115, https://doi.org/10.1029/2017JF004395.

Rounce, D. R., Khurana, T., Short, M. B., Hock, R., Shean, D. E., and Brinkerhoff, D. J. (2020). Quantifying parameter uncertainty in a large-scale glacier evolution model using Bayesian inference: application to High Mountain Asia. Journal of Glaciology, 66(256), 175-187, https://doi.org/10.1017/jog.2019.91.

Sakai, A., and Fujita, K.: Contrasting glacier responses to recent climate change in high-mountain Asia, Scientific reports, 7(1), 1-8, https://doi.org/10.1038/s41598-017-14256-5, 2017.

Sanjay, J., Krishnan, R., Shrestha, A. B., Rajbhandari, R., and Ren, G. Y.: Downscaled climate change projections for the Hindu Kush Himalayan region using CORDEX South Asia regional climate models, Advances in Climate Change Research, 8(3), 185-198, https://doi.org/10.1016/j.accre.2017.08.003, 2017.

Scherler, D., Wulf, H., and Gorelick, N. (2018). Global assessment of supraglacial debris-cover extents. Geophysical Research Letters, 45(21), 11-798, https://doi.org/10.1029/2018GL080158.

Shea, J. M., and Immerzeel, W. W.: An assessment of basin-scale glaciological and hydrological sensitivities in the Hindu Kush–Himalaya, Annals of Glaciology, 57(71), 308-318, https://doi.org/10.3189/2016AoG71A073, 2016.

Shean, D. E., Bhushan, S., Montesano, P., Rounce, D. R., Arendt, A., Osmanoglu, B.: A systematic, regional assessment of high mountain Asia glacier mass balance, Frontiers in Earth Science, 7, 363, https://doi.org/10.3389/feart.2019.00363, 2020.

Sherpa, S. F., Wagnon, P., Brun, F., Berthier, E., Vincent, C., Lejeune, Y., ... Sinisalo, A.: Contrasted surface mass balances of debris-free glaciers observed between the southern and the inner parts of the Everest region (2007–15), Journal of Glaciology, 63(240), 637-651, https://doi.org/10.1017/jog.2017.30, 2017.

Singh, P., and Kumar, N.: Effect of orography on precipitation in the western Himalayan region. Journal of Hydrology, 199(1-2), 183-206, https://doi.org/10.1016/S0022-1694(96)03222-2, 1997.

Singh, P., Kumar, N., Arora, M.: Degree–day factors for snow and ice for Dokriani Glacier, Garhwal Himalayas, Journal of Hydrology, 235(1-2), 1-11, https://doi.org/10.1016/S0022-1694(00)00249-3, 2000.

Singh, P., Haritashya, U. K., Ramasastri, K. S., and Kumar, N.: Diurnal variations in discharge and suspended sediment concentration, including runoff-delaying characteristics, of the Gangotri Glacier in the Garhwal Himalayas, Hydrological Processes: An International Journal, 19(7), 1445-1457, 10.1002/hyp.5583, 2005.

Singh, A. T., Sharma, P., Sharma, C., Laluraj, C. M., Patel, L., Pratap, B., ... Thamban, M.: Water discharge and suspended sediment dynamics in the Chandra River, Western Himalaya, Journal of Earth System Science, 129(1), 1-15, https://doi.org/10.1007/s12040-020-01455-4, 2020.

Soncini, A., Bocchiola, D., Confortola, G., Minora, U., Vuillermoz, E., Salerno, F., ... Diolaiuti, G.: Future hydrological regimes and glacier cover in the Everest region: The case study of the upper Dudh Koshi basin, Science of the Total Environment, 565, 1084-1101, https://doi.org/10.1016/j.scitotenv.2016.05.138, 2016.

Soruco, A., Vincent, C., Rabatel, A., Francou, B., Thibert, E., Sicart, J. E., and Condom, T.: Contribution of glacier runoff to water resources of La Paz city, Bolivia (16 S), Annals of Glaciology, 56(70), 147-154, 10.3189/2015AoG70A001, 2015.

Sunako, S., Fujita, K., Sakai, A., and Kayastha, R. B.: Mass balance of Trambau Glacier, Rolwaling region, Nepal Himalaya: in-situ observations, long-term reconstruction and mass-balance sensitivity, Journal of Glaciology, 65(252), 605-616, 10.1017/jog.2019.37, 2019.

Tarantola, A. Inverse problem theory and methods for model parameter estimation, Society for Industrial and Applied Mathematics, https://doi.org/10.1137/1.9780898717921, 2005.

Tawde, S., Kulkarni, A., and Bala, G.: An estimate of glacier mass balance for the Chandra basin, western Himalaya, for the period 19842012, Annals of Glaciology, 58(75pt2), 99-109, 10.1017/aog.2017.18, 2017.

Van Tiel, M., Kohn, I., Van Loon, A. F., and Stahl, K.: The compensating effect of glaciers: Characterizing the relation between interannual streamflow variability and glacier cover. Hydrological Processes, 34(3), 553-568, https://doi.org/10.1002/hyp.13603, 2020.

Van Tiel, M., Stahl, K., Freudiger, D., and Seibert, J.: Glacio-hydrological model calibration and evaluation. Wiley Interdisciplinary Reviews: Water, 7(6), e1483, https://doi.org/10.1002/wat2.1483, 2020.

Van Tiel, M., Van Loon, A. F., Seibert, J., and Stahl, K.: Hydrological response to warm and dry weather: do glaciers compensate?. Hydrology and Earth System Sciences, 25(6), 3245-3265, https://doi.org/10.5194/hess-25-3245-2021, 2021.

Vano, J. A., Das, T., Lettenmaier, D. P.: Hydrologic sensitivities of Colorado River runoff to changes in precipitation and temperature, Journal of Hydrometeorology, 13(3), 932-949, https://doi.org/10.1175/JHM-D-11-069.1, 2012.

Vijay, S., and Braun, M.: Elevation change rates of glaciers in the Lahaul-Spiti (Western Himalaya, India) during 2000–2012 and 2012–2013. Remote Sensing, 8(12), 1038, https://doi.org/10.3390/rs8121038, 2016.

Vincent, C., Ramanathan, Al., Wagnon, P., Dobhal, D. P., Linda, A., Berthier, E., Sharma, P., Arnaud, Y., Azam, M. F., Jose, P. G., and Gardelle, J.: Balanced conditions or slight mass gain of glaciers in the Lahaul and Spiti region (northern India, Himalaya) during the nineties preceded recent mass loss, The Cryosphere, 7, 569–582, https://doi.org/10.5194/tc-7-569-2013, 2013.

Werder, M. A., Huss, M., Paul, F., Dehecq, A., and Farinotti, D.: A Bayesian ice thickness estimation model for large-scale applications. Journal of Glaciology, 66(255), 137-152, https://doi.org/10.1017/jog.2019.93, 2020.

Wang, R., Liu, S., Shangguan, D., Radic, V., Zhang, Y.: Spatial heterogeneity in glacier mass-balance sensitivity across High Mountain Asia, Water, 11(4), 776, https://doi.org/10.3390/w11040776, 2019.

Zhang, L., Su, F., Yang, D., Hao, Z., and Tong, K.: Discharge regime and simulation for the upstream of major rivers over Tibetan Plateau, Journal of Geophysical Research: Atmospheres, 118(15), 8500-8518, 10.1002/jgrd.50665, 2013.

Zhao, Q., Zhang, S., Ding, Y. J., Wang, J., Han, H., Xu, J., ... Shangguan, D.: Modeling hydrologic response to climate change and shrinking glaciers in the highly glacierized Kunma Like River Catchment, Central Tian Shan, Journal of Hydrometeorology, 16(6), 2383-2402, https://doi.org/10.1175/JHM-D-14-0231.1, 2015.

Zheng, H., Zhang, L., Zhu, R., Liu, C., Sato, Y., Fukushima, Y.: Responses of streamflow to climate and land surface change in the headwaters of the Yellow River Basin. Water Resources Research, 45(7), https://doi.org/10.1029/2007WR006665, 2009.